機　　密
CONFIDENTIAL

國立臺灣大學 研究成果專利申請表

本校案號：02A-150601
(由產學合作總中心填寫)

請勾選以下兩種選項中的一種（請參考第 2-3 頁的詳細說明）： 2015.05.06 版

□「先期專利申請案」 (即美國 **Provisional Application**，技術已公開者請勿申請)；

■「後期專利申請案」；針對本發明，是否已向校方提出「先期專利申請案」？■是，□否

計畫合作機構	科技部 (請填寫本申請案所屬之經費來源，如：科技部、經濟部、農委會等)	□利用本校資源 (勾選本項則無需填計畫名稱及編號)
計畫名稱及編號	中孔洞二氧化矽奈米粒子與血液(MOST 103-2113-M-002 -021 -MY2) (請填寫衍生本申請案之所有計畫，並附核定清單或契約書影本；填寫空間請自行調整)	
計畫合作期限及金額	自 2014 年 12 月 1 日 至 2016 年 7 月 31 日; 共新台幣 4,606,000 元整	
發明名稱	Silica Nanoparticle-Mediated Delivery of Antibody, Enzymes or Proteins into Cells (非為原計畫名稱，請為本申請案技術內容訂定名稱)	
擬申請之國家	□中華民國 ■美國 □其他：__ provisional application number: 62034282, 62034181, 62034192 <請參見附件五>	

※附件 (請依「先期專利申請案」或「後期專利申請案」，準備所需文件；標示＊者為必須提供)
※請於『研究成果專利申請表』的 **word** 檔填寫完成後，務必 **email** 給所屬之本中心窗口。
(關於本中心各人員執掌暨聯絡資訊，請參連結 **http://ord.ntu.edu.tw/CIAC/Responsibilities.aspx**)

「先期專利申請案」	□＊技術推廣表(附件一)；□＊技術分類表(附件二) □＊國立臺灣大學研究成果基本資料表(附件三) □＊送至美國 USPTO 之技術文件 (可直接用論文，但盡量完整地揭露欲保護範圍技術內容，建議以英文撰寫，可包括圖式；無頁數或格式限制)
「後期專利申請案」	□＊技術推廣表(附件一)；☑＊技術分類表(附件二) ☑＊國立臺灣大學研究成果基本資料表(附件三) ☑＊費用分攤協議書(附件四)；☑＊研究成果專利構想揭露書(附件五) ☑相關文獻陳報表(附件六) ☑計畫經費核定清單(科技部計畫)或研究計畫補助合約書影本(非科技部計畫) □已公開或預計公開之相關文件(若於附件三第四點勾選公開或預計公開者) □學位論文口試保密同意書影本 □與本案相關之文獻資料影本

提 案 人：　　(簽章)　　單　位：國立台灣大學化學系

提案日期：104 年 6 月 5 日　　職　　稱：教授

敬　　陳

系 主 任　理學院化學系 編審 簡佳慧　理學院化學系 系主任 楊吉水(代)

院　　長　理學院 秘書 李明騏　理學院 院長 劉緒宗(甲)

研發處（產學合作總中心）
擬依專利申請程序辦理
研發處產學合作總中心智權管理師 陳慧蘭 104.06.08
研發處產學合作總中心主任 胡文聰

研　發　長

A. 「先期專利申請案」(provisional application)之優點：

1. 可藉最少的經費、在最短的時間內(會議/論文發表/口試前)，先獲得多個國家(中華民國、美國、大陸及 PCT 國家)最基本的專利保護(申請日及申請號)。若準備僅申請中華民國專利亦可用美國「先期專利申請案」。
2. 無須準備正式的專利說明書或專利範圍(claim)，只要以自行準備的技術資料 (可採論文格式，請以英文撰寫)，寄送紙本至美國 USPTO 後即完成申請 (USPTO 收到文件日為「先期專利申請案」正式申請日)。所需繳納費用僅有郵資與美國政府規費(2014 年 7 月時為 US$130[1])；亦可採線上申請。
3. 能有更充裕的時間，與專利事務所討論，精心設計極重要之「後期專利申請案」的專利範圍，以確保最大專利利益(專利範圍不會過於狹窄)。
4. 可視近期技術發展趨勢、產業變化、與廠商洽談技轉等結果，來決定是否一年內送「後期專利申請案」，如此亦能使有限的資源發揮更高的效益。(建議「先期專利申請案」送件後約 9 個月後啟動「後期專利申請案」，以確保專利品質) 。

註 1：美國政府規費約 2~3 年變動一次，各項規費請以美國 USPTO 官網公布之數據為準。

B. 其他「先期專利申請案」注意事項:

1. 「後期專利申請案」(即正式之專利案)單是申請費用 (台灣案約 NT$40,000，美國案約 NT$100,000)，為龐大的投資，連同答辯、年費、其他可能發生之程序一同計算，中華民國發明案約新台幣 15-35 萬/件、美國發明案約 60-85 萬/件。
2. 請先自行向美國官方提出美國「先期專利申請案」(詳細步驟請見下頁)，再向產學合作總中心提出「國立臺灣大學研究成果專利申請表」 (本申請表；第一頁請勾選「先期專利申請案」) 。
3. 如先提出美國「先期專利申請案」，並於一年內提出「後期專利申請案」，可引用美國「先期專利申請案」的申請日為優先權日，因此，於前/後期專利案申請日之間所出現的其他人技術文件，仍不會干擾「後期專利申請案」獲准專利權。
4. 「先期專利申請案」寄到美國 USPTO 後，USPTO 不會直接審核(僅歸檔)，等到收到「後期專利申請案」後(若「後期專利申請案」主張「先期專利申請案」之優先權日期)，於「先期專利申請案」申請日起 18 個月時，一併公開先/後期專利申請案。
5. 「先期專利申請案」的技術資料，可包含多種技術內容，不受限於一發明一申請；而當技術研究陸續地出現進展時，亦可逐一地申請更多「先期專利申請案」，於最早提出申請之美國「先期專利申請案」申請日一年內申請「後期專利申請案」時，可主張各件「先期專利申請案」的優先權。
6. 若有新增技術內容，請確保美國「先期專利申請案」的發明人與「後期專利申請案」的發明人之間，至少一人重疊。
7. 網頁 http://www.uspto.gov/patents/resources/types/provapp.jsp 有更詳細說明，請參考。
8. 網頁 http://www.uspto.gov/web/offices/ac/qs/ope/fee010114.htm 可查閱最新美國先期專利的申請規費清單；根據 2014 年 5 月美國專利商標局的網站資料，小實體(small entity，含個人)申請美國先期專利的規費為美金 130 元。如需要最新規費資訊，亦可於 google 上搜尋『USPTO Provisional application filing fee』。
9. 可向 USPTO 申請註冊帳號(Customer Number)，往後即可至 USPTO 的網頁上綜覽申請過

的所有美國專利案;相關內容請參以下網頁連結 http://www.uspto.gov/patents/ebc/about.jsp。

C. 以紙本方式，向美國 USPTO 申請「先期專利申請案」：

1. 請備好英文之「先期專利申請案」技術文件，可直接用論文為技術文件，但盡量完整地揭露欲保護範圍技術內容，列印成紙本，一旦送出後不能修改；
2. 請至網頁 http://www.uspto.gov/forms/sb0016.pdf 填寫 cover sheet、列印，並簽名 (此網頁為 Provisional Application for Patent Cover Sheet)；
3. 請至 http://www.uspto.gov/forms/2038-fill.pdf 填寫信用卡單、列印，並簽名(此網頁為 Instructions for Completing the Credit Card Payment Form)；
4. 請將上述各紙本文件郵寄至以下地址：

   Commissioner for Patents
   P. O. Box 1450
   Alexandria, VA 22313-1450
   USA

註 1: 「先期專利申請案」正式申請日為美國 USPTO 收到文件日。USPTO 日後並將 filing receipt (含 Application Number) 寄至案件中所提供之郵寄地址。

註 2: 寄出 USPTO 後務必提出「國立臺灣大學研究成果專利申請表」(本申請表)，產學合作總中心將協助技轉。

D. 以網路操作，向美國 USPTO 申請「先期專利申請案」：

1. 尚未註冊者，請至網頁 https://efs.uspto.gov/EFSWebUIUnregistered/EFSWebUnregistered；模擬練習可先至網頁 http://www.uspto.gov/ebc/portal/sandbox/efs0-3-0.htm。
2. 已通過數位認證者，請至網頁 https://efs.uspto.gov/TruePassSample/AuthenticateUserLocalEPF.html；模擬練習可先至網頁 http://www.uspto.gov/ebc/portal/sandbox/efs0-4-0.htm。
3. 關於常見問題(FAQs)，請參考網頁 http://www.uspto.gov/ebc/efs_faq.htm。

註: 網路完成申請後，務必提出「國立臺灣大學研究成果專利申請表」(本申請表)，產學合作總中心將協助技轉。

附件一、技術推廣表(含以下兩頁之中、英文表單)

為協助技術移轉，是否有意願與本中心合作推廣本技術※?

□是(本中心將於技術交易網或各媒合會上發佈此資料)；

■否(原因_使用本技術衍生新創公司_；若有意願使用本技術衍生新創公司者，可勾否)。

※依專利法第七條規定，提案人之各專利案的專利申請權及專利權，皆屬本校所有。

發明名稱

(以下內容一頁為限，不可揭露關鍵技術內容；填表完成後請刪除此行)

發明人： OOO 教授
單　位： 國立臺灣大學　OOO 學系/研究所
簡　歷：(可列出相關連結，例如系所、研究室網頁)

請放任一代表照片
(不可揭露技術內容)

市場及需求:

技術摘要(含成果):

優勢:

競爭產品:

專利現況:
(1)本技術已有相關專利（中華民國專利申請號:XXXX；美國專利證號: XXX)。
(2)本研究團隊具有數十年研究經驗…
(3)其他…

聯絡方式(請不用填):
臺大產學合作總中心
Tel: 02-3366-9945,　E-mail: ntuciac@ntu.edu.tw

本資料僅供國立臺灣大學專利/技術申請使用，嚴禁使用全部或部分內容於其他用途。若有疑問請與我們聯繫，我們將盡力協助您。

Title of Invention

(Below is limited to 1-page only; be careful not to disclose vital technology content. Please delete these words when the document is finished)

PI： Prof. XXX
Department of XXX, National Taiwan U.

Experience:

An interesting **photo** related to your technology
(be careful not to disclose key technology)

Market Needs:

Our Technology:

Strength:

Competing Products:

Intellectual Properties:

Contact (do not need to fill out):

Center for Industry-Academia Cooperation, NTU
Tel: 02-3366-9945, E-mail: ntuciac@ntu.edu.tw

This information herein is intended for potential license of NTU technology only. Other usage of all or portion of this information in whatever form or means is strictly prohibited. Kindly contact us and we will help to achieve your goal the best we can.

請務必填寫此附件

機　密
CONFIDENTIAL

附件二、技術分類表

(請依技術本質勾選(可複選)或於其他(請自填)欄位填入適當類別；分類結果將置於網頁)

一階	二階	三階
生醫農健	農業	□植物種苗□動物種苗□生物農藥□生物肥料□抗病/蟲/逆境性□生物整治□品種權□生物機電□組織培養□觀賞□發酵□基因轉殖□糧食□蔬菜□天然物利用□遺傳育種□森林學□獸醫學□其他(請自填)_____
	醫療器材	□診斷與監測用器材□體外診斷用器材□手術與治療用器材□輔助與彌補用器材其他類醫療器材□疼痛管理器材□低/非侵入性器材□預防疾病與健康促進之設備及用品□其他(請自填)_____
	篩選平台	□抗體□生物晶片□細胞分析□組合式分子生物□組合化學□高通量藥物篩選技術(HTS)噬菌體展示技術□蛋白酶□藥物篩選□標靶藥物□其他(請自填)_____
	藥物	□止痛藥□麻醉劑□血管生成□消炎□抗生素□抗體■抗癌□抗真菌□antisense□抗病毒■細胞凋亡■細胞訊息□中樞神經系統□疾病模型 ■藥物輸送□生育□基因治療□賀爾蒙■免疫治療□發炎□新陳代謝□天然物□病原體□胜肽□前驅藥物■蛋白質□RNAi□小分子藥物幹細胞□疫苗□病毒□傷口癒合□其他(請自填)_____
	基因體學	□allele□生物資訊學□cDNA□DNA□流行病學□EST□基因□基因型□homologue□isogene□基因庫□微陣列/微陣列分析軟體□藥物基因體學□聚合酶□多型性□定位選殖□蛋白質體學□受體□RNA□標靶驗證□基因轉殖動物□其他(請自填)_____
	研究工具	□抗體□細胞株□色層分析□細胞培養□定向分子演化□DNA / RNA 定序□DNA / RNA 合成□電泳□酵素□裝置□表現系統□雜交□老鼠模式□寡核苷酸合成□PCR 檢測□蛋白酶□蛋白質定序□蛋白質合成□試劑□RNAi□光譜□載體□其他(請自填)_____
	技術	□抗體□生物晶片□顯影劑□DNA 探針□造影成像□分子標記□放射性同位素□檢測技術□其他(請自填)_____
電資通光	電子光電	□光資訊技術□光電半導體技術□平面顯示技術□背光技術□軟性電子技術□光學技術(含鏡片材料)□電子及光電構裝技術□矽基半導體技術□電磁/光電訊號檢測□奈米電子技術□其他(請自填)_____
	資訊通訊	□有線網路□語音□資訊安全□監控□網際網路電話相關技術(VoIP) □Web 相關技術□智慧型資訊系統□無線通訊技術□射頻辨識技術及應用(RFID)□環境控制與感知技術□數位視/音訊與多媒體技術□光通訊技術□電子商務□嵌入式系統技術□其他(請自填)_____
機能材化	材料化工	□添加劑□觸媒□塗料/塗佈□電化學□石墨烯□導電高分子□塑料/聚合/複合材料□化學/生物分析■奈米材料□半導體材料/製程□物料改質□超導體□分散均勻化□光學薄膜 □其他(請自填)_____
	能源環工	□替代/生質能源□燃料電池□化學/生物分析□高電功率□碳氫化合物□儲能□節能減碳□太陽能/電池□海洋工程□醫學/診斷/器械/儀器□環境整治□土木工程□水利工程□感測/量測方法/系統□其他(請自填)_____
	機械儀設	□機械元件/裝置/設備□分析儀器□光學/激光機器人□顯微技術□導航(GPS)□光譜儀□超音波□電腦輔助設計/檢測□圖像處理□環境感測/感應器□生理訊號感測□致動器□微機電/元件/系統□微控制□其他(請自填)_____
其他(請自填)		

請務必填寫此附件

機　　密
CONFIDENTIAL

附件三、國立臺灣大學研究成果基本資料表

本校案號：02A-150601 (陳慧蘭)
(由產學合作總中心填寫)

提案日期：中華民國 104 年 6 月 5 日

一、發明名稱	中文：氧化矽奈米材料輸送抗體, 酵素或蛋白質 英文：silica nanoparticle-mediated delivery of antibody, enzymes or proteins into cells					
二、提案人	姓名	牟中原	服務單位	台大化學系	職稱	教授
	電話	02-33665251	e-mail	cymou@ntu.edu.tw		
三、欲申請專利之目的(可複選)	■有意以本案為關鍵技術，新創事業，而需專利保護； □已有廠商願意技轉本案技術 / 洽談技轉事宜中； 廠商名稱 / 聯絡窗口：＿＿＿＿＿＿＿＿ 電話：＿＿＿＿＿＿＿＿ □本案之對應專利為科技產業之基礎專利(essential patent)，例如通訊產業或網際網路的通訊規格； □本技術所開發出之物品/設備，在結構上具創新性，故需專利保護，才能透過結構解析，來對照專利權之範圍，以確認是否被侵權。					
四、權利歸屬	■臺大 □共有：與＿＿＿＿＿共有，共有比例為＿＿＿%：＿＿＿% (請填寫共有機構名稱) (臺　大　：共有機構) □其他：＿＿＿＿＿＿					
五、本申請案是否已公開?	※根據中華民國及美國專利法規定，凡案件於申請前已見於刊物或公開發表（含學位論文口試、學位論文電子全文及電子書目資料(含摘要)上網、學位論文紙本全文上架、學術刊物發表、學術研討會發表、媒體報導、上課講習、公開演講、參加展覽會、競賽發表…等公開事項），需於其事實發生後六個月內（若申請美國案為12個月內）提出申請方符合申請要件。 □是(請續填以下) ■否，未來預計會公開(請續填以下) □否 請註明公開事實及日期(若有多次公開，請條列) (1) small 2014, 10, 4785 (August 26, 2014) (2)＿＿＿＿＿＿ ※學位論文口試視同公開，若採取以下手段，則可能認為不算公開(1)口試會議不以網路公告(2)口試時聽眾不能自由進出，避免對不特定人士揭露技術(3)所有參加口試會議者(含口試者)簽署保密同意書(請提供影本一份)。 ※學位論文繳交提醒：論文電子全文、電子書目資料(含摘要)及紙本論文若於網路上或圖書館供人查詢或閱覽也算是公開，若欲採取保密措施需於(1)本校電子學位論文服務系統上傳論文電子全文時，於系統上勾選電子全文延後公開，並另行填寫「學位論文延後公開申請書」向圖書館申請(2)電子書目資料(含摘要)及(3)紙本論文延後公開(注意：若於公開後才向圖書館申請延後公開，則仍以原公開日期為公開日) ※為維持申請專利內容之新穎性，請盡量在申請前勿公開相關內容。若已公開或預計公開請檢附已公開或預計公開之相關文件。					

六、建議檢索關鍵字	中文： 氧化矽奈米材料, 中孔洞氧化矽奈米材料 CONFIDENTIAL 英文：silica nanoparticle + (protein, enzyme, antibody), mesoporous silica nanoparticle

七、發明人

※發明人欄位填寫說明：

(1)發明人超過四位時，請自行複製發明人欄位使用。

(2)發明人請填寫實際的發明人，參酌美國專利實務上的認定，所謂發明人必須是對發明概念之形成及至少一項申請專利範圍之標的有所貢獻之人，才能稱為發明人。美國專利法規定，若列名之發明人未有發明之事實，則不得取得專利；若發明人記載錯誤，且可證明有「欺瞞之意圖」，則此專利權無法主張權利（單純接受指示，依所設計之實驗完成實驗結果者、提出需求者、提出產品缺點者等無實質貢獻者，不能算是發明人）。

(3)未來收益分配之有功人員不限於此專利申請案所列之實際發明人。

1	姓名	(中文/英文) 牟中原/ Chung-Yuan Mou		
	服務單位	國立台灣大學化學系	職稱	教授
	國　籍	■中華民國 □其他：_____	身份證字號或護照字號	F102827685
	e-mail	cymou@ntu.edu.tw	電話	+886-2-33665251
	聯絡地址	106 台北市大安區學府里 18 鄰基隆路 3 段 30 巷 5 弄 10 號		
2	姓名	(中文/英文) 陳奕平/ Yi-Ping Chen		
	服務單位	Academia Sinica	職稱	博士後研究員
	國　籍	■中華民國 □其他：_____	身份證字號或護照字號	F123456542
	e-mail	d96223202@ntu.edu.tw	電話	+886-2-33665895
	聯絡地址	基隆市中山區中和路 85 巷 5 弄 27 號		
3	姓名	(中文/英文) 吳思翰/ Si-Han Wu		
	服務單位	Academia Sinica	職稱	博士後研究員
	國　籍	■中華民國 □其他：_____	身份證字號或護照字號	L122994887
	e-mail	R94223056@ntu.edu.tw	電話	+886-2-33665233

		聯絡地址	42047 台中市豐原區大明路 169 號 6 樓		
七、發明人(續)	4	姓名			
		服務單位		職稱	
		國　籍		身份證字號或護照字號	
		e-mail		電話	
		聯絡地址			

八、本申請案所屬技術領域別與可能應用範圍	本申請案所屬技術領域	藥物輸送
	可能應用範圍(產業或產品)	(此欄位類似於技術推廣表中的『市場與需求』) 作為蛋白質藥物及小分子藥物輸送載體, 醫藥產業
	※本專利應用之可行性及潛在授權廠商： (1)本專利之技術與該國現有產品或技術之競爭性如何？ (2)依據本專利之產品或製程進入該國市場的可行性如何？ (3)若有任何公司曾與您接洽或詢問過相關技術，亦請提供。	
	國家/地區	**應用可行性及潛在授權廠商建議（請列舉並以文字說明）**
	中華民國	
	美國	
	其他	

※發明人專利費用分攤說明：

經本研發成果所衍生之相關權益義務，將依「國立臺灣大學研究發展成果及技術移轉管理要點」辦理，有關專利申請費用之分攤及研發成果權利金及衍生利益之分配如要點第七點及第十二點，條文如下；另請留意，若有積累專利費用未繳納，將影響您後續申請新專利案之權益：

七、專利申請費用之分攤

經研發處審議通過據以申請專利者，專利申請之申請費、證書費、第一期專利年費、事務所手續費及其他依法令應繳納之專利規費等(以下簡稱專利申請費用)，依下列原則分攤：

(一)申請之專利費用分攤比率如下：由校方負擔45%、發明人負擔50%、發明人所屬單位(院系所)負擔5%；有資助機關補助案件者，校方負擔55%、發明人負擔40%、發明人所屬單位(院系所)負擔5%。遇有特殊情況，研發長經財務副校長同意後，籌組專案小組評議，評議結果報請校長核准後，專利費用最高得由本校負擔95%。

(二)本校依規定向資助機關申請補助專利相關費用而獲准後，其所申請之補助費用，由本校運用於研發成果管理維護及推廣。

(三)研究經費由基金會或私人企業提供者，亦得由經費提供者自行向有關專利主管機關申請，本校不負擔相關費用，其智慧財產權之歸屬仍應依第二點規定辦理。

(四)院系及相關單位不願負擔專利申請費用者，其負擔部分由學校負責，其相對技轉收入(如授權金及衍生利益金)歸屬學校。

(五)專利審查過程中發明人有提出申復、補充、修正、答辯等情事者，前三次必要之費用依第一款規定比率分攤；第四次以上費用，由發明人先自行負擔，最後確認獲准通過時，再依第一款規定比率分攤。

發明人若欲放棄繳納應負擔之專利費用，應載明理由向專利承辦單位提出申請並經核准得放棄繳納。專利承辦單位催繳仍未繳納者亦視同放棄繳納。放棄繳納之專利案件數將列入後續審核專利申請之事由。

經財務處同意之投資案件，有關費用分擔於簽陳校長同意後，不適用前項規定。

十二、研發成果權利金及衍生利益之分配

技轉收入於扣除回饋資助機關、校方及發明人成本（含專利申請費用、年費）之部分後，依下列比率分配：

(一)專利授權案件，其分配比率如下：校方20%、發明人70%、發明人所屬單位(院系所)10%。

(二)第七條第一項第一款第三目之案件分配比率如下：發明人所屬單位（院系所）10%、發明人20%、其餘70%由校方及發明人分配比率依雙方出資比率決定之。

(三)非專利授權件案，其分配比率如下：校方40%、發明人50%，發明人所屬單位10%。

本校研究中心向本校專利承辦單位提出專利授權案件之申請並經核准，得進行技轉類建教合作之推廣，若有收入則優先扣除15%提供予本校研究中心後，其餘由各單位依前項第一款之比例分配。

經財務處同意之投資案件，有關費用分配於簽陳校長同意後，不適用前項規定。

申請「後期專利案」者請填寫此附件，申請「先期專利案」者無須填寫

機　密
CONFIDENTIAL

附件四、國立臺灣大學研究成果申請專利費用分攤協議書

一、 請填寫案件資訊--

1. 發明名稱：Silica Nanoparticle-Mediated Delivery of Antibody, Enzymes or Proteins into Cells
2. 本校編號（由產學合作總中心填寫）：02A-150601
3. 申請國別： 美國

二、 ※發明人專利申請費用分攤說明：

1. 專任教師在校任職期間，利用計畫或校方資源完成之研究而衍生之發明或其他智慧財產權，其智慧財產權為本校所有。
2. 依「國立臺灣大學研究發展成果及技術移轉管理要點」第七點第一款及第十二點，本案發明人之專利申請費用分攤及權益收入分配比例如下，各比例亦將隨日後此管理要點或資助機關補助方案的變動而改變。
3. **請留意，若有積累專利費用未繳納，將影響您後續申請新專利案之權益。**

◎有資助機關補助之案件

專利費用分攤比率方案		※專利申請費用分攤（%）			※權益收入分配比例（%）		
		校	發明人	院系所	校	發明人	院系所
資助機關審核	通過	55	**40**	5	20	**70**	10
	未通過	45	**50**	5	20	**70**	10

◎無資助機關補助之案件

專利費用分攤比率方案	※專利申請費用分攤（%）			※權益收入分配比例（%）		
	校	發明人	院系所	校	發明人	院系所
	45	**50**	5	20	**70**	10

4. 專利申請過程中發明人應協助 STRIKE 系統登錄，以及答辯(含申復、補充、修正…等)之辦理；前三次答辯之必要費用依上述比率分攤，第四次以上費用，由發明人先自行負擔，於確認獲准通過時，再憑原始單據並依第一款規定比率分攤。
5. 由發明人負擔之各項專利費用，以及未來可能衍生的權利金與利益分配，皆由提案人為支付或領取的代表，請提案人務必配合相關作業流程。
6. 專利案總費用(新台幣；含各階段)概估：中華民國發明案約 15-35 萬/件、美國發明案約 60-85 萬/件。

三、 本案經發明人同意依上述專利費用分攤比率辦理。

提案人：[signature] 2015/6/15 （簽章+日期）

申請「後期專利案」者請填寫此附件，申請「先期專利案」者無須填寫

機　密
CONFIDENTIAL

附件五、國立臺灣大學研究成果專利構想揭露書

(※此附件將提供給事務所，以利其了解本案技術內容；可自行擴充欄位)

一、專利類別	■發明　□新型(於美國亦將提出發明專利申請)　□設計 ※ 發明，指利用自然法則之技術思想之創作。 新型，指利用自然法則之技術思想，對物品之形狀、構造或裝置之創作。 設計，指對物品之全部或部分之形狀、花紋、色彩或其結合，透過視覺訴求之創作。
二、申請國家及理由	□中華民國　■美國　□其他：_____ ※本校專利申請審查原則：以中華民國、美國兩國為優先考量，若欲申請其他國別(含歐盟、PCT)，則需請發明人依擬申請之國別提供以下三種狀況之說明文件，並經校方審查程序，如未附相關資料則無法審查。 (1)有廠商願意技術移轉；(2)有授權潛力；(3)市場評估良好。
三、發明背景及內容	(1) 發明所欲解決之問題： 係指申請專利之發明或新型所要解決先前技術中存在的問題。
	蛋白質藥物(蛋白質、酵素、抗體等)所面臨共同問題為蛋白質藥物本身不易進入細胞而導致藥效降低，或者在輸送過程中因降解而失去藥效。此外在修飾蛋白質藥物過程中為了避免破壞蛋白質結構因此提高樣品處理上的困難。
	(2) 解決問題之技術手段： 即欲獲得專利保護之主要技術特徵，請條列本案相較於先前技術具有創新、進步或功效等獨特技術部分，做為撰寫申請專利範圍之參考。
	利用特定的氧化矽奈米材料輸送變性蛋白質，使其在細胞內部自行恢復蛋白質活性的方式，可不需考慮蛋白質藥物其結構是否因修飾過程而改變。並可利用氧化矽奈米材料有效包覆蛋白質藥物提高其細胞輸送效率並且保護蛋白質藥物於輸送過程中不被降解，並可將其輸送至細胞內特定位置。
	(3) 對照先前技術之功效： 係指前述技術手段所產生的技術效果。(等同於技術推廣表『本技術之優勢』)
	1. 可利用中孔洞氧化矽奈米材料輸送變性之蛋白質藥物，使其進入細胞後再恢復活性，此方法可不需考慮蛋白質藥物其結構是否因修飾過程而改變。 2. 利用氧化矽奈米空心球，可於合成過程中一步且有效包覆蛋白質藥物提高其細胞輸送效率並且保護蛋白質藥物於輸送過程中不被降解。 3. 利用與抗體結合後之中孔洞氧化矽奈米材料大小特性，將特定細胞傳導分子阻擋於特定胞器外。
四、本發明之實施方式	**請舉出至少一項關於本發明之較佳實施方式或具體實施例，可配合圖示說明，使所屬技術領域中具有通常知識者能了解其內容並可據以實施。** (本項可於本表格說明或以技術文件、論文等代替)

Synthesis of Enzyme Encapsulated Nanospheres

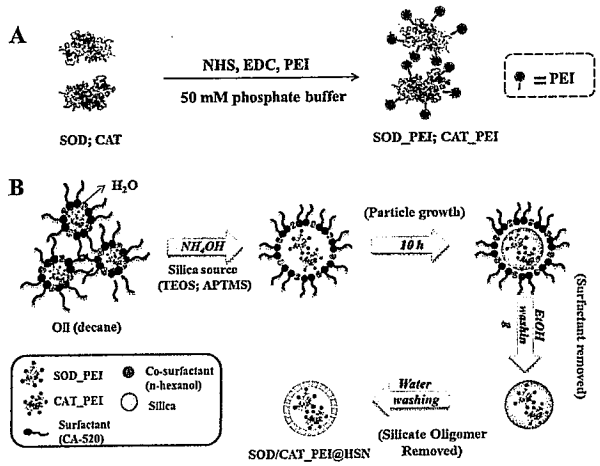

Cascade Reaction of Superoxide Dismutase and Catalase Encapsulated HSN Acting Inside Cells

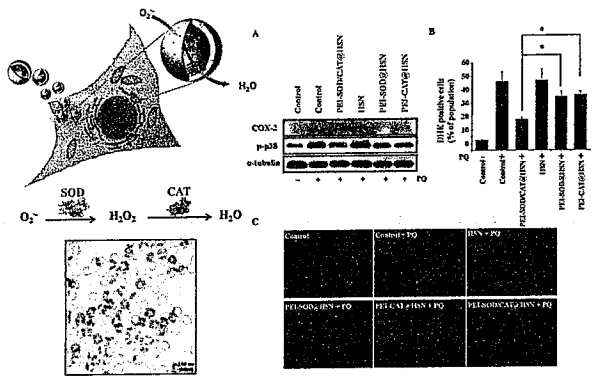

〈請參見附件五〉

附件六、相關文獻陳報表

※請條列與本案技術領域相關之文獻，包含但不限於提案人或發明人之相關專利、論文等。

1. 專利(包含申請中及已獲證案件，請至少寫出申請國別及申請案號/獲證號)

(1) 美國 8409876

(2) 美國 8642356

(3) 美國 7332351

(4) 美國 7955866

2. 其他(該文獻若無法於網路上輕易取得，請檢附相關文件影本 1 份)

(1) H. Sies, *Eur J. Biochem.*, **1993**, *215*, 213-219.
(2) D. M. Vriezema, P. M. Garcia, N. Sancho Oltra, N. S. Hatzakis, S. M. Kuiper, R. J. Nolte, A. E. Rowan and J. C. van Hest, *Angew. Chem. Int. Ed.*, **2007**, 46, 7378-7382.
(3) F. Lu, S. H. Wu, Y. Hung and C. Y. Mou, *Small*, **2009**, 5, 1408-1413.
(4) S. H. Wu, C. T. Tseng, Y. S. Lin, C. H. Lin, Y. Hung and C. Y. Mou, *J. Mater. Chem.*, **2011**, *21*, 789-794.
(5) C. G. Palivan , O. Fischer-Onaca , M. Delcea , F. Itel , W. Meier , *Chem. Soc. Rev.* **2012** , *41* , 2800.
(6) S. H. Wu, C. Y. Mou and H. P. Lin, *Chem. Soc. Rev.*, **2013**, *42*, 3862-3875.
(7) Y. P. Chen, C. T. Chen, Y. Hung, C. M. Chou, T. P. Liu, M. R. Liang, C. T. Chen and C. Y. Mou, *J. Am. Chem. Soc.*, **2013**, *135*, 1516-1523
(8) Y. Chen, P. Xu, H. Chen, Y. Li, W. Bu, Z. Shu, Y. Li, J. Zhang, L. Zhang, L. Pan, X. Cui, Z. Hua, J. Wang, L. Zhang and J. Shi, *Adv. Mater.*, **2013**, 25, 3100-3105.
(9) F. P. Chang, Y. P. Chen and C. Y. Mou, *Small*, **2014**, ***10***, 4785-4795.
(10) Y. Chen, H. R. Chen and J. L. Shi, *Acc. Chem. Res.*, **2014**, 47, 125-137.

Electronic Acknowledgement Receipt	
EFS ID:	19797958
Application Number:	62034181
International Application Number:	
Confirmation Number:	9584
Title of Invention:	Catcher in the Rel: Nanoparticles-Antibody Conjugate as NF-kB Nuclear Translocation Blocker. Mesoporous silica nanoparticle (MSN) of size around 50 nm contains fluorescence dye FITC in the pores for tracking while its surface is functionalized with NF-kB p65 antibody and Tat protein. The nuclear localization MSN-Tat conjugates eventually converge toward perinuclear region, where the p65 specific antibody perform the targeting and catching against active NF-kB p65 effectively.
First Named Inventor/Applicant Name:	Chung-Yuan Mou
Correspondence Address:	Chung-Yuan Mou - No. 1, Sec. 4, Roosevelt Road - Taipei - 10617 TW +886233668205 -
Filer:	Chung-Yuan Mou
Filer Authorized By:	
Attorney Docket Number:	
Receipt Date:	07-AUG-2014
Filing Date:	
Time Stamp:	06:15:57
Application Type:	Provisional

Payment information:

Submitted with Payment	yes
Payment Type	Credit Card
Payment was successfully received in RAM	$130

RAM confirmation Number	9167
Deposit Account	
Authorized User	

File Listing:

Document Number	Document Description	File Name	File Size(Bytes)/ Message Digest	Multi Part /.zip	Pages (if appl.)
1		Provisional_NFkB.pdf	7906262 3f80e5d614f4e1f2fe5f77f06bf1bd280c7622f5	yes	34

Multipart Description/PDF files in .zip description		
Document Description	**Start**	**End**
Specification	1	9
Drawings-other than black and white line drawings	10	25
Specification	26	34

Warnings:

Information:

2	Provisional Cover Sheet (SB16)	SB16_NFkB_MSN.pdf	341214 8651a50940d959cf04504ff3d2dd0f32dc351dda	no	3

Warnings:

This is not a USPTO supplied Provisional Cover Sheet SB16 form.

Information:

3	Fee Worksheet (SB06)	fee-info.pdf	30498 33dbbd718a7c6f79975527a1486abe500fa8c9f5	no	2

Warnings:

Information:

Total Files Size (in bytes):	8277974

Electronic Acknowledgement Receipt

EFS ID:	19801187
Application Number:	62034282
International Application Number:	
Confirmation Number:	1068
Title of Invention:	Intracellular implant of enzymes-in-hollow silica nanosphere for protein therapy: Cascade system of superoxide dismutase and catalase. Polyethyleneimine grafted superoxide dismutase and catalase encapsulated in hollow silica nanosphere as a nanoreactor gives cascade reaction converting superoxide ion into water and oxygen. Upon uptaken in Hela cell, the nanoreactor protects the cell against reactive oxygen species.
First Named Inventor/Applicant Name:	Chung-Yuan Mou
Correspondence Address:	Chung-Yuan Mou - No. 1, Sec. 4, Roosevelt Road - Taipei - - TW - -
Filer:	Chung-Yuan Mou
Filer Authorized By:	
Attorney Docket Number:	
Receipt Date:	07-AUG-2014
Filing Date:	
Time Stamp:	12:29:35
Application Type:	Provisional

Payment information:

Submitted with Payment	yes
Payment Type	Credit Card
Payment was successfully received in RAM	$130

RAM confirmation Number	11283
Deposit Account	
Authorized User	

File Listing:

Document Number	Document Description	File Name	File Size(Bytes)/ Message Digest	Multi Part /.zip	Pages (if appl.)
1		Provisionl_Enzyme_HSN.pdf	8512701 aa73137ec811bd7a9cd566e17c070bdd6252 24dfe	yes	44

Multipart Description/PDF files in .zip description

Document Description	Start	End
Specification	1	20
Drawings-other than black and white line drawings	21	22
Specification	23	44

Warnings:

Information:

2	Provisional Cover Sheet (SB16)	SB16_Enzyme_HSN.pdf	369523 52e74c2da6079523296c5192fd2cb57a347 cffbb	no	3

Warnings:

This is not a USPTO supplied Provisional Cover Sheet SB16 form.

Information:

3	Fee Worksheet (SB06)	fee-info.pdf	29390 b32bb6f7b89b5ac6856b7fec9a8a18b25eb 190ca	no	2

Warnings:

Information:

Total Files Size (in bytes):	8911614

Electronic Acknowledgement Receipt

EFS ID:	19798052
Application Number:	62034192
International Application Number:	
Confirmation Number:	9799
Title of Invention:	Co-delivery of Superoxide Dismutase (SOD) and Glutathione Peroxidase (GPx) by Using Mesoporous Silica Nanoparticles. FMSN was first synthesized and modified by silane tether (NTA-Ni) to form FMSN-NTA-Ni. The fusion proteins of His-tagged TAT-hSOD and His-tagged TAT-hGPx were constructed and expressed by using genetic engineering method. Finally, the two fusion proteins are conjugated on the MSN surface respectively through the Ni and His-tagged interaction to compose sequential ROS scavengers.
First Named Inventor/Applicant Name:	Chung-Yuan Mou
Correspondence Address:	Chung-Yuan Mou - No. 1, Sec. 4, Roosevelt Road - Taipei - - TW - -
Filer:	Chung-Yuan Mou
Filer Authorized By:	
Attorney Docket Number:	
Receipt Date:	07-AUG-2014
Filing Date:	
Time Stamp:	07:53:02
Application Type:	Provisional

Payment information:

Submitted with Payment	yes
Payment Type	Credit Card
Payment was successfully received in RAM	$130

RAM confirmation Number	9271
Deposit Account	
Authorized User	

File Listing:

Document Number	Document Description	File Name	File Size(Bytes)/ Message Digest	Multi Part /.zip	Pages (if appl.)
1		Provisional_NIHis_MSN.pdf	10391295 870e16cee784ad2e51bcd9ca9039660362b75e39	yes	58

Multipart Description/PDF files in .zip description		
Document Description	**Start**	**End**
Drawings-other than black and white line drawings	1	1
Specification	2	58

Warnings:

Information:

2	Provisional Cover Sheet (SB16)	SB16_NiHis_MSN.pdf	756363 7e2cfca7c7c1d4e0240bd6744ccfba5a9d52ef1a	no	3

Warnings:

This is not a USPTO supplied Provisional Cover Sheet SB16 form.

Information:

3	Fee Worksheet (SB06)	fee-info.pdf	30205 9d7134de1e8686bb4b1d54b3df4a2e62b74508f1	no	2

Warnings:

Information:

Total Files Size (in bytes):	11177863

Journal Name

RSCPublishing

ARTICLE

Catcher in the Rel: Cytosol Delivery of Nanoparticles-Antibody Conjugate as NF-κB Nuclear Translocation Blocker

Cite this: DOI: 10.1039/x0xx00000x

Received 00th January 2012,
Accepted 00th January 2012

DOI: 10.1039/x0xx00000x

www.rsc.org/

Yi-Ping Chen[†,‡], Si-Han Wu[†,‡], Chien-Tsu Chen[§], Fan-Ching Chien[‖], Peilin Chen[‡] and Chung-Yuan Mou[*,†]

Transcription factor complex NF-κB (p65/p50) is localized to the cytoplasm by its inhibitor IκBα. Upon activation, the Rel proteins p65/p50 are released from IκBα and transported through nuclear pore to effect many gene expressions. While inhibitions of up or down stream signal pathway are often ineffective due to cross talks and compensations, direct blocking of the Rel proteins p65/p50 has long been proposed as a potential target for cancer therapy. In this work, a nanoparticle/antibody complex targeting NF-κB is employed to catch the Rel protein p65 in perinuclear region and thus blocking the translocation near the nuclear pore gate. TAT peptide conjugated on mesoporous silica nanoparticles (MSN) help non-endocytosis cell-membrane transducing and converge toward perinuclear region, where the p65 specific antibody performed the targeting and catching against active NF-κB p65 effectively. The size of the p65 bound nanoparticle becomes too big to enter nucleus. The new approach of anti-body therapy targeting on transcription factor with "nucleus focusing" and "size exclusion blocking" effects of the antibody-conjugated nanoparticle is general and may be applicable to modulating other transcription factors.

Introduction

A key step in all eukaryotic signal transduction mechanisms involves the translocation of transcriptional factors through nuclear pores from the cytoplasm into the nucleus to respond the request of many physiological purposes, with gene expression, signal transduction, and cell cycle progression.[1-3] The processing of nuclear localization is usually induced by trafficking from the cell surface via signaling cascade. In principle, transcription factors are attractive drug targets because regulating their activity provides a general method to alter physiology and pathology at gene level.[4] However, modulating transcription factors have been considered to be undruggable because transcription factors (TF) are not readily amenable to small molecular regulations.[5] On the other hand, delivering an antibody against TF through a properly designed nanocarrier for blocking specific transcription factor could be a viable and versatile approach for its regulation. In fact, this strategy has been employed in nature in virus attack of host. For example, STAT1 transcription factor residing in cytosol can be rapidly transported through a nonclassical import mechanism into nucleus to establish an antiviral state. Ebola virus VP24 protein can precisely block the specialized STAT1 import to abolish the downstream antiviral activities.[6] In this paper, we propose a general method of using surface-designed nanoparticle to deliver antibody to block the function the transcription factor, NF-κB.

Nuclear factor-κB (NF-κB) is a transcription factor that enters the nucleus and initiates transcription of large number downstream effector genes involved in regulation of immune responses, inflammation and metastasis.[7, 8] The majority of NF-κB exists as a heterodimer of p65/p50 Rel proteins sequestered in the cytosol by binding to inhibitory IκBα proteins. The IκBα protein dissociates from NF-κB upon activation and p65/p50 then translocate into nucleus to start gene expression.[9, 10] Many types of human tumors have constitutively active NF-κB owing to dys-regulated signals.[11-13] Thus, inhibition of NF-κB activation and its signaling pathways could provide promising new approaches for cancer chemotherapeutics.[14] Blocking NF-κB as a targeting therapy can cause tumor cells to stop proliferating, or to become more sensitive to the action of anti-tumor agents. Strategies based on inhibitors for blocking NF-κB have been reported in either upstream or downstream of the signaling pathway.[15] More than 700 different inhibitors of NF-κB have been reported until now[11]. However, inhibitors lacking high specificity to target protein or interferences from other signaling systems of the parallel crosstalk make the inhibition of NF-κB as a therapeutic target often ineffective. Our

This journal is © The Royal Society of Chemistry 2013

approach is to block the translocation of the specific transcription factor Rel protein p65/p50 near nuclear pore, which is analogous to catching a goal-tending ball in a soccer game, with a p65-antibody-nanoparticle construct.

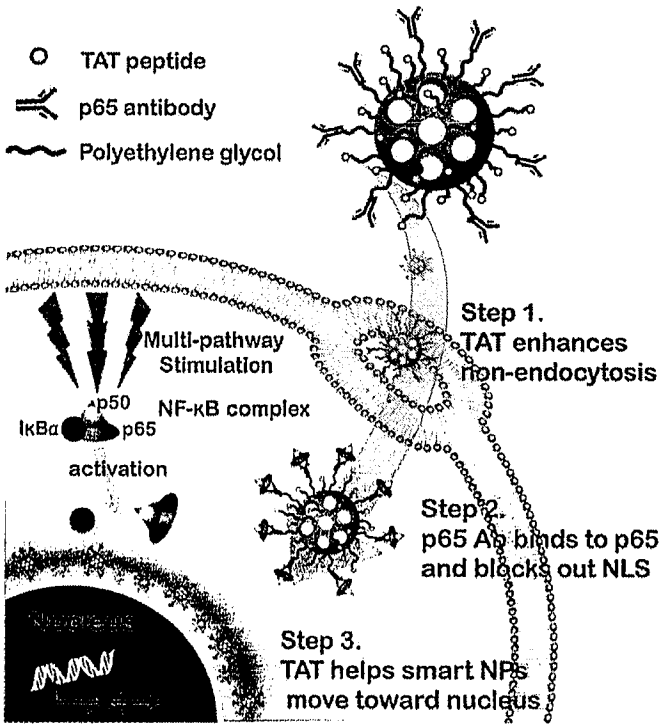

Scheme 1. Schematic representation of a smart nanoparticle consisting of mesoporous silica nanoparticle (MSN) with surface functionalization of NF-κB p65 antibody and TAT transducing peptide. The smart nanoparticles move near nuclear membrane and block nuclear translocation of the activated p65 through steps 1-3.

In reported antibody-based nanotechnology, cellular surface type of antibody such as human epidermal growth factor receptor 2 (HER2) is conjugated onto nanoparticles to block or target surface antigens through immunogenic recognition for detection/diagnosis, imaging and therapy.[16, 17] However, there have yet no report on an antibody therapy for blocking the nuclear transduction event in cytoplasm because antibody have severe permeability problems to enter cell except by using cargo delivery or cell-penetrating peptide (CPP) conjugated antibody.[18] We deal with this problem with conjugation of the p65 antibody on CPP-conjugated nanoparticles. The CPP-nanoparticle construct will be an effective nanocarrier for carrying the p65 antibody into cell and focusing towards nucleus to catch the Rel protein p65. For the nanocarrier, we choose mesoporous silica nanoparticle (MSN)[19-21] for its easy functionalization, large internal volume for building multifunctionality.

Cell-penetrating peptide (CPP) such as transactivator of transcription (TAT) peptide containing a small region of YGRKKRRQRRR have been explored for promoting cell penetration and nuclear targeting in vitro.[18, 22] TAT peptides conjugated with nanoparticles has been shown to guide the cell nuclear entering. TAT-functionalized small MSN has been used to carry cancer drug into cell nucleus for effective cancer therapy.[23-25] In our case, we will have MSNs large enough that they are blocked from entering the nuclear pore.

To achieve a specific inactivation of the Rel protein p65 released from activated NF-κB, we take a strategy of MSN/p65 antibody/TAT peptide complex targeting NF-κB (Scheme I). The hypothesis is the p65 antibody conjugated nanoparticles can effectively catch and block the translocation of NF-κB in the perinuclear region. This would avoid much of the cross-talks in upstream events. The size of the MSNs-cargo complex (> 40 nm) would be too big to enter the nuclear pores. Through size hindrance, one thus intercepts and blocks the translocation of p65. Taking advantage of the natural propensity of TAT for nuclear targeting[23-25] and p65 antibody for catching p65 in perinuclear region, we show this smart nanoparticle can successfully block TNF-induced NF-κB p65 activity in HeLa cells and inhibits cell proliferation in HNSCC cells. Our method is general in that the chemical functionalization of the nanoparticle can be varied to target other transcription factors, or focusing on other intracellular organelle to develop new type of intracellular antibody therapy.

Results and discussion

To synthesize the functionalized MSN (Figure 1a), we first attached amine groups on the surface of MSN by reacting with 3-aminopropyltrimethoxysilane (APTMS) to form MSN-APTMS with an average loading of nitrogen content of APTMS at 2.6 wt % by elemental analysis.

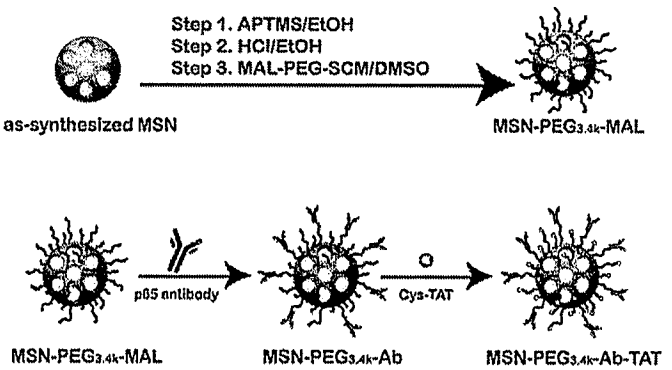

Figure 1. Schematic illustration of the conjugation of NF-κB p65 antibody and Cys-TAT peptide to the surface functionalized MSN. (a) Synthesis of MSN with heterobifunctional PEG crosslinker (MAL-PEG-SCM). The MAL-PEG-SCM crosslinker contains a succinimidyl moiety which reacts with the amine group of MSN-APTMS. (b) The MAL-end of MSN-PEG reacted with the thiol groups of the antibody and Cys-TAT peptide.

In order to immobilize p65 antibody on MSN, we chose two polyethylene glycol (PEG) crosslinkers with different lengths, MAL-PEG_{2k}-SCM and MAL-$PEG_{3.4k}$-SCM, to MSN-APTMS. The MAL-PEG-SCM crosslinkers reacted with the amine groups of MSN-APTMS through an active succinimidyl link to obtain the MSN-PEGs (MSN-PEGs: MSN-PEG_{2k}, MSN-$PEG_{3.4k}$). Elemental analysis indicated that the APTMS of MSN-APTMS to PEG_{2k} ratio is about 8 : 1 and the APTMS to APTMS-$PEG_{3.4k}$ ratio is about 14 : 1. We have checked MSN-

This journal is © The Royal Society of Chemistry 2012

PEG_{2k} and MSN-$PEG_{3.4k}$ did not induce the nuclear p65 expression without TNF-α treatment, which is comparable to the control (Figure S1). Also, PEG-modified MSNs did not affect or interfere with the p65 activation by TNF-α in HeLa cells. Since different lengths of PEG did not cause any undue result, we continued the particle functionalization by using the MSN-$PEG_{3.4k}$.

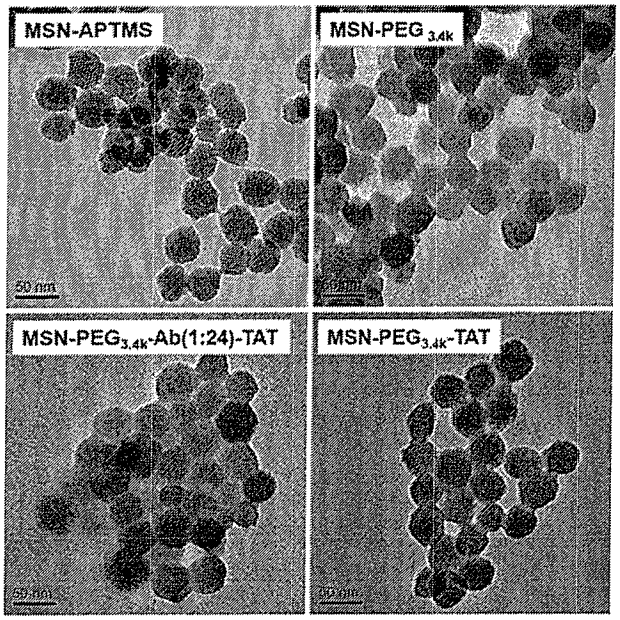

Figure 2. TEM images of the nanoparticles.

Table 1. DLS measurements of particle size.

	MSN-APTMS	MSN-$PEG_{3.4k}$	MSN-$PEG_{3.4k}$-Ab(1:24)-TAT	MSN-$PEG_{3.4k}$-TAT
Size (nm)	340 ± 8	157 ± 6	242 ± 7	274 ± 10
PDI	0.27	0.25	0.39	0.32

For evaluation of immunological efficiency, the p65 antibody was covalently immobilized with the MAL-end of MSN-$PEG_{3.4k}$ in different ratios (1:6, 1:12, 1:24) via C-S binding. (Figure 1b) After the p65 antibody conjugation, the Cys-TAT peptide was conjugated to fill up the free MAL-end of MSN-$PEG_{3.4k}$. MSN-$PEG_{3.4k}$ without antibody coupling was also directly conjugated with Cys-TAT as a control. The physical properties of the nanoparticles were characterized by nitrogen adsorption- desorption isotherms, powder X-ray diffraction (XRD), FT-IR, TEM, dynamic light scattering (DLS) and zeta potential (Figure 2, S2-6 and Table 1, S1). Basically, these data gives well- ordered and surfactant-extracted mesoporous structure. TEM micrograph shows that the MSN particles possess well-ordered mesoporous structure and the average particle size from TEM images are ~ 40 nm (Figure 2). DLS-determined size indicates slight aggregation in solution (Table 1) giving size of antibody-TAT conjugated nanoparticle at about 240 nm, but they are still suspended well enough to give long term stability. MSNs of this size range have been reported for good cell-uptake.[19]

We then study the effectiveness of the designed nanoparticle for binding to activated NF-κB p65. Activated NF-κB was evaluated by using a monoclonal antibody that selectively recognizes p65/p50 dimer in activated NF-κB. Immunocytochemical staining and Western blotting analysis were performed for the purpose. An *in vitro* pull-down assay was used to test the immunological activity of p65 antibody attached to the nanoparticle toward its antigen (Figure 3a).

The result indicated that the free p65 level after pull down decreases as the amount of antibody content in the MSN-$PEG_{3.4k}$-Ab-TAT increases. The epitope of the antibody on the MSN does exhibit pull-down activity against p65. We further examined the cell viability of the MSN-$PEG_{3.4k}$-Ab-TAT by WST-1 assay and found MSN-$PEG_{3.4k}$-Ab-TAT has no significant cytotoxicity (Figure S7).As shown in Figure 3b, western blotting was carried out to quantify the p65 level in HeLa cells. After the treatment, the cell lysates were harvested for the p65 level in nucleus and cytoplasm. The western blot results indicated that MSN-$PEG_{3.4k}$-Ab-TATs did not induce any nuclear translocation of p65 without TNF-α. However, under the TNF-α treatment, a significant increase of p65 level appeared in the nucleus in absence of MSN-$PEG_{3.4k}$-Ab-TATs. Once the MSN-$PEG_{3.4k}$-Ab-TATs with different amount of conjugated antibody were added, the level of nuclear p65 gradually reduced with increasing amount of antibody. Both MSN-$PEG_{3.4k}$-Ab(1:12)-TAT and MSN-$PEG_{3.4k}$-Ab(1:24)-TAT show obvious suppression of the p65 translocation to nucleus, whereas MSN-$PEG_{3.4k}$-TAT did not prevent the TNF-α inducing nuclear p65 translocation. Hence, MSN-$PEG_{3.4k}$-Ab-TAT shows the specificity and effectiveness to block NF-κB p65 nuclear translocation through immunogenic binding. To verify the western blotting results, confocal microscopy (Figure S8) imaged that MSN-$PEG_{3.4k}$-Ab-TAT and MSN-$PEG_{3.4k}$-TAT have efficiently entered into HeLa cells. After induction with TNF-α, p65 translocated from the cytosol to the nucleus, as seen in the overlapping blue and red images (from purple to pink) in the "merge" column. We found that the p65 nuclear translocation after TNF-α treatment was dramatically inhibited by MSN-$PEG_{3.4k}$-Ab-TAT as the stained p65 protein (red) remaining in the cytosol. Meanwhile, for MSN-$PEG_{3.4k}$-TAT, the Rel p65 protein, was visibly present in the nucleus. The yellow images showed the co-localization of MSN-$PEG_{3.4k}$-Ab-TAT (green) and p65 (red). Both MSN-$PEG_{3.4k}$-Ab(1:12)-TAT and MSN-$PEG_{3.4k}$-Ab(1:24)-TAT strongly suppressed the translocation of p65 according to the Alexa-568 staining in nucleus. MSN-$PEG_{3.4k}$-TAT, on the other hand, exhibited little actions on p65 translocation. These data also show that the TAT peptide on MSNs helps the cargo delivered in cytosol and thus the p65 antibody retains its activity. In addition, the amount of p65 antibody functionalized onto MSN-$PEG_{3.4k}$-Ab(1:24)-TAT was determined by a fluorescence spectrometric method to be 28 μg/mg. The amount of TAT peptide functionalized onto MSN-$PEG_{3.4k}$-Ab(1:24)-TAT was 1.9×10^{-5} mol/g.

This journal is © The Royal Society of Chemistry 2012

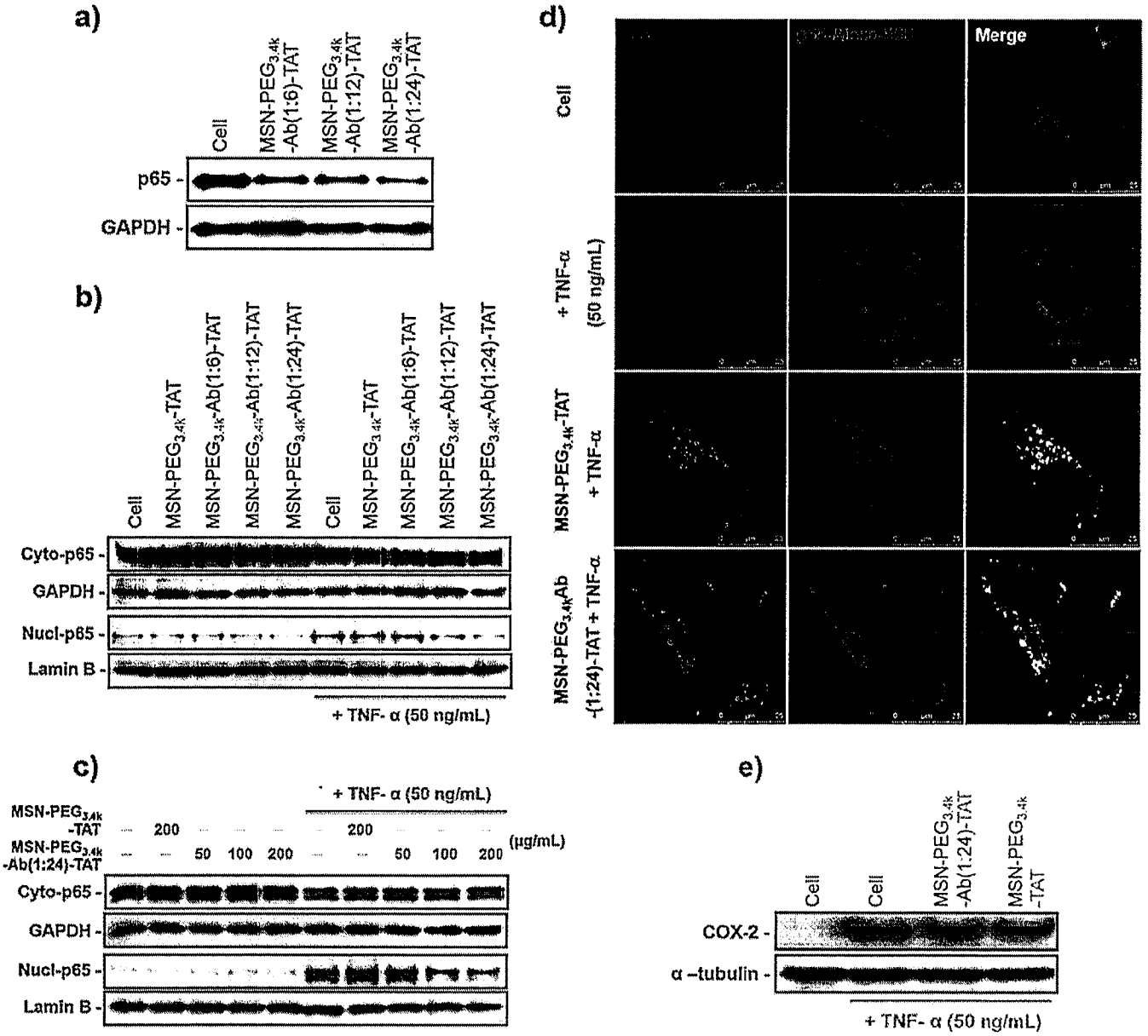

Figure 3. In vitro pull-down assay and MSN-PEG3.4k-Ab-TAT blocks NF-κB p65 nuclear translocation and thus inhibits the NF-κB p65 downstream protein expression. (a) For in virto pull-down assay to test p65 antibody activity on the surface of MSN, the MSN-PEG3.4k-Ab-TAT (100 μg/mL) was incubated with total cell lysates in vitro. Then the supernatant was assayed the p65 expression level by Western blotting. HeLa cells were treated with MSN-PEG3.4k-TAT or MSN-PEG3.4k-Ab-TAT for 4 h at a dose of (b) 100 μg/mL, (c) 50-200 μg/mL and (d-e) 200 μg/mL. After the delivery, the cells were stimulated with or without 50ng/mL TNF-α for another 0.5 h (b-d) or 4 h (e). (b-c) Western blotting assay of the level of cytosolic and nuclear p65. d) Intracellular localization of p65 using confocal laser scanning microscopy (CLSM) imaging. DAPI (blue), Alexa-568-labeled anti-p65 antibody (red), and FITC-MSN (green). (e) Cell lysates were analyzed for the level of COX-2 protein (NF-κB down-regulator) by Western blotting assay. GAPDH, Lamin B and α-tubulin were used as a loading control.

Further dose-dependence study of the blockage in Figure 3c shows nuclear p65 level decreased in with increase of the concentration of MSN-$PEG_{3.4k}$-Ab(1:24)-TAT. The results of CLSM (Figure 3d and Figure S9) also confirmed that less p65-Alexa 568 staining pattern in nucleus when increasing the concentration of MSN-$PEG_{3.4k}$-Ab(1:24)-TAT. In contrast, MSN-$PEG_{3.4k}$-TAT exhibited some interaction with p65 in the cytosol (yellow) but had no subsequent inhibition on p65 translocation. NF-κB has been implicated in tumor promotion and cell survival/proliferation as mediated by the cell proliferation genes and cell survival genes (e.g., BCL-2 and COX-2).[26-28] Thus, we further examined COX-2 which was activated and mediated by the p65 nuclear translocation. Fig. 3e shows COX-2 protein was present under TNF-α (50 ng/mL) treatment. When we increased the delivery of MSN-$PEG_{3.4k}$-Ab(1:24)-TAT, the TNF-α induced COX-2 protein (NF-κB down-regulator) expression significantly decreased. But, MSN-$PEG_{3.4k}$-TAT could not decrease the TNF-α induced COX-2 protein expression.

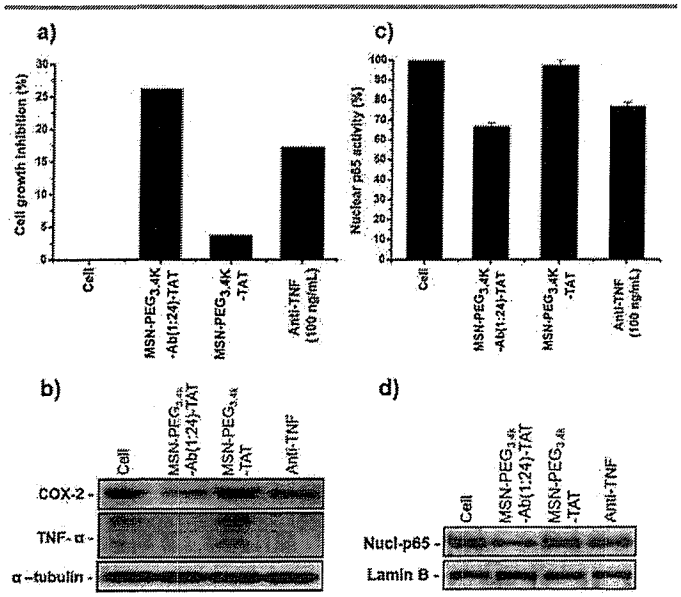

Figure 4. MSN-PEG3.4k-Ab(1:24)-TAT efficiently inhibits the proliferation and decreases nuclear NF-κB p65 activity in HNSCC cells. HNSCC cells were treated with 200 μg/mL of MSN-PEG3.4k-TAT, MSN-PEG3.4k-Ab(1:24)-TAT or anti-TNF antibody (100 ng/mL) for 4 h. Then, cells were further incubated in culture medium for 72 h. (a) Cells growth inhibition was assayed by WST-1 method. (b) HNSCC cell lysates were prepared and analyzed for COX-2 and TNF-α protein level using western blotting assay. α-tubulin was used as a loading control. (c) For nuclear NF-κB p65 activity, nuclear extracts were prepared, and the nuclear NF-κB p65 activity was measured by ELISA kit with anti-65 antibodies. ELISA was performed as described in methods section and the experiment was repeated three times. (d) At the same condition as (c), the same nuclear extracts were also analyzed for NF-κB p65 protein level using western blotting assay. Lamin B was used as a loading control.

To show that the strategy could be useful to inhibit tumor cell proliferation for possible future tumor therapy, head and neck squamous cell carcinoma (HNSCC, SSC-4) cell line with constitutive activation of NF-κB mediated through the TNF pathway was studied.[29-31] To evaluate whether the HNSCC growth was affected by MSN-$PEG_{3.4k}$-Ab(1:24)-TAT due to inhibiting p65 translocation, we delivered MSN-$PEG_{3.4k}$-Ab(1:24)-TAT into HNSCC. The proliferation of HNSCC cells were determined by using WST-1 assay. We found that MSN-$PEG_{3.4k}$-Ab (1:24)-TAT had a significant inhibition (26%) at a concentration of 200 μg/mL, whereas MSN-$PEG_{3.4k}$-TAT (200 μg/mL) had almost no effect. In a separate positive control experiment, anti-TNF antibody shows an inhibition of proliferation in HNSCC cells[31] at near 17% level as a comparison (Figure 4a). We further examine the protein levels of cell survival/proliferation gene COX-2 and TNF-α by Western blotting. Both play important roles in tumor promotion. As expected, HNSCC cells exhibited higher basal levels of COX-2 and TNF-α (Figure 4b). When treated with MSN-PEG3.4k-Ab(1:24)-TAT and anti-TNF-α antibody, both COX-2 and TNF-α decreased, with COX-2 decreasing more. Figure 4c show that the nuclear NF-κB p65 activity by ELISA assay was significant inhibited in cells treated with MSN-$PEG_{3.4k}$-Ab(1:24)-TAT (65%) or anti-TNF antibody (72%) as compared with controls. The nuclear NF-κB p65 protein levels were decreased in the treatment of either MSN-$PEG_{3.4k}$-Ab(1:24)-TAT or anti-TNF antibody. MSN-$PEG_{3.4k}$-Ab(1:24)-TAT had shown a greater inhibition than anti-TNF antibody (Figure 4d). These explains that MSN-$PEG_{3.4k}$-Ab(1:24)-TAT inhibited the growth of HNSCC cells.

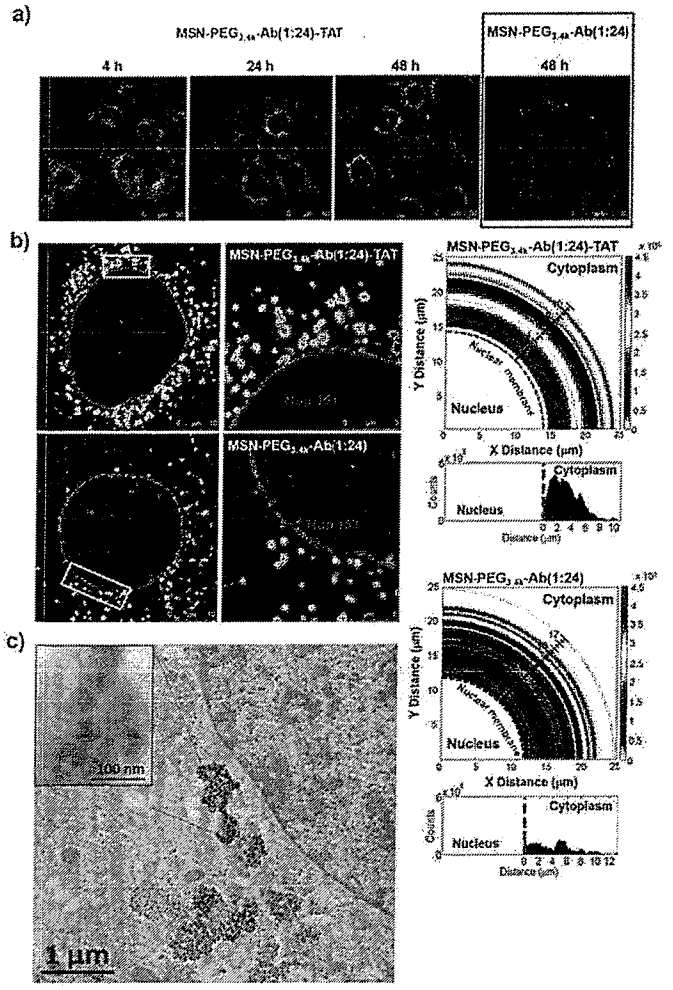

Figure 5. MSN-PEG3.4k-Ab(1:24)-TAT focus toward nucleus due to TAT peptide interacting with importins. (a) HNSCC cells were treated with 200 μg/mL of MSN-PEG3.4k-Ab(1:24) or MSN-PEG3.4k-Ab(1:24)-TAT for 4, 24 and 48 h, and the images were observed by using confocal laser scanning microscopy (CLSM). After the delivery for 48 h, the cells were fixed for the following experiments. (b) The nuclear pore was stained with anti-Nup 153 antibody and imaged by confocal laser scanning microscopy. Alex-568-labeled anti-Nup 153 antibody (pink), and FITC-MSN (green). Then, the fluorescence intensity of the FITC-MSN with a distance relative to the nuclear membrane was summated to plot the distribution map by Matlab program. The color bar indicated the value of fluorescence intensity. The histogram showed distribution of fluorescence intensity along the radial axis. (Details are in the methods section) (c) Bio-TEM images of MSN-PEG3.4k-Ab(1:24)-TAT.

To observe whether the nanoparticles MSN-$PEG_{3.4k}$-Ab(1:24)-TAT focus toward nucleus, the localizations of MSN-$PEG_{3.4k}$-Ab(1:24)-TAT after cellular uptake for 4, 24, and 48 h were examined by confocal microscopy (Figure 5a). As time evolved, we see a gradual focusing of the distribution of MSN-$PEG_{3.4k}$-Ab(1:24) to closer distance from nuclear membrane.(e.g. thinner green rings around the nucleus). Cellular nuclear pore protein of Nup153 was stained and imaged. As shown in Figure 5b, most of MSN-$PEG_{3.4k}$-Ab(1:24)-TAT were localized at

perinuclear region in the cytoplasm from the co-localization images of MSN-$PEG_{3.4k}$-Ab(1:24)-TAT (green, FITC) and nuclear pore[32] (pink, Nup153 staining). Comparatively, much less particles were located immediately near the nucleus when treated with MSN-$PEG_{3.4k}$-Ab(1:24). We analyzed statistically the fluorescence intensity distribution of MSNs at different distance from nuclear membrane. Figure 5b (right) showed the fluorescence intensity distributions of MSN-$PEG_{3.4k}$-Ab(1:24) and MSN-$PEG_{3.4k}$-Ab(1:24)-TAT in cytoplasm. MSN-$PEG_{3.4k}$-Ab(1:24)-TAT (Figure 5b. Upper right) are concentrated at distances 250 nm to 4.5 μm from the nuclear membrane (red-colored region), while the control experiment of MSN-$PEG_{3.4k}$-Ab(1:24) shows much diffuse distribution far away from nucleus (Figure 5b. Lower right). Bio-TEM analysis also revealed that MSN-PEG3.4k-Ab(1:24)-TAT exhibited near perinuclear region and formed a ring structure surrounding the nucleus (Figure 5c and Figure S10). Apparently, TAT peptides enhanced MSN-$PEG_{3.4k}$-Ab(1:24)-TAT focusing in the surrounding of the nucleus. The reason could be due to TAT on the MSN-$PEG_{3.4k}$-Ab(1:24)-TAT which binds with the receptors, importin α and β, leading to interaction with nuclear pore complex (NPC) on nuclear surface.[24, 33, 34] It is clear that MSN-$PEG_{3.4k}$-Ab(1:24)-TAT was blocked from entering the nucleus with a possible mechanism of size hindrance. A tendency from TAT-conjugated nanoparticle toward nuclear translocation may have directed a "chemotaxis" style movement to defense/action/trap near the nuclear pore for increasing the inhibition of p65 nuclear translocation. We also note that the NF-κB p65 antibody recognized the epitope at dimerization domain of NF-κB p65 near nuclear localization sequence (NLS) which may well block the interaction between NLS and NPC due to steric hindrance as illustrated in the scheme in Figure S11. All these factors, nuclear focusing, size blocking, binding to Rel protein and NLS hindrance, are designed in the conjugated nanoparticle MSN-$PEG_{3.4k}$-Ab(1:24)-TAT. Further improvements over the present nanomaterials might well make this new approach more effective including. One could try more careful adjustment of surface functionalization to decrease aggregation and improve dispersion of the MSNs in medium.[35, 36] Secondly, optimization of spacer in linking nuclear focusing peptide for enhanced intracellular active transport along microtubule. Recent theoretical study on this issue may help us better design.[37] Finally, one could use better design of cell-penetration peptides such as unnatural peptides for the purpose. Recently, we have shown enhanced non-endocytosis cellular uptake of MSNs by replacing shortened side chains of amino acids in TAT.[38]

Conclusions

In conclusion, a novel concept in nanoparticles-based therapy for intervening cell signaling pathways was demonstrated. With anti-p65 antibody-TAT conjugated MSN designed as a translocation blocker, the nanoparticles were successful in attacking NF-κB p65 and blocking p65 nuclear translocation. In cell biology, signal transduction mechanisms are involved in many physiological or biological functions. Most often, proteins nuclear translocation is the key step in altering gene expression for normal cell functions. This work is the first demonstration using nanoparticles as nuclear translocation blocker for the regulation of cell signaling transduction. It could be generalized to other nuclear translocations of protein in tuning the involved signal pathway. Our results open a new strategy for future applications of nanoparticles in medicine.

Experimental section

Materials and Methods

All chemicals were purchased from commercial suppliers (Acros, Sigma-Aldrich and Merck) and were used without further purification. MSN and amine-functionalized MSN (MSN-APTMS) were synthesized according to our previously reported methods.[39]

Conjugation of PEG linker with MSN-APTMS (MSN-PEG2k, MSN-PEG3.4k).

The heterobifunctional MAL-PEG-SCM (SCM: Succinimidyl Carboxy Methyl ester, one type of NHS ester ; MAL: Maleimide) linkers were covalently conjugated onto MSN-APTMS through the NHS group by reacting with the amine group on MSN-APTMS. PEG2k (41.63 mg) or PEG3.4k (70.78 mg) linkers was dissolved in DMSO solution (9 mL) followed by the addition of MSN-APTMS (30 mg) in 3 mL DMSO. Subsequently, 0.3 mL PBS solution was added to the above solution, and the mixture was stirred for 24 h at room temperature. The products, called MSN-PEG2k or MSN-PEG3.4k, were collected by centrifugation and washed with ethanol several times to eliminate unreacted PEG linkers. Finally, MSN-PEG2k and MSN-PEG3.4k were dispersed in ethanol and stored at room temperature.

Immobilization of NF-κB p65 antibody on MSN-$PEG_{3.4k}$.

NF-κB p65 antibody (12 μg, 24 μg, and 48 μg) (Santa Cruz Biotechnology, Santa Cruz, CA) was mixed and incubated with MSN-$PEG_{3.4k}$ (1 mg) in the conjugation buffer (0.1x PBS) at 4 °C for 18 h. After that, the p65 antibody conjugated MSN-$PEG_{3.4k}$ (MSN-$PEG_{3.4k}$-Ab) were isolated by centrifugation and washed several times with 0.1x PBS. Afterwards, the MSN-$PEG_{3.4k}$-Ab were suspended and stored in 0.1x PBS at 4 °C.

Synthesis of TAT conjugated MSN-$PEG_{3.4k}$-Ab.

Cys-TAT peptide was covalently conjugated onto MSN-$PEG_{3.4k}$-Ab through the –SH group. In this work, 1.14 mg Cys-TAT was dissolved in 0.1x PBS (1 mL) followed by the addition of 1mg MSN-$PEG_{3.4k}$-Ab in 0.1x PBS (1 mL). The mixture was then stirred at 4°C for 18 h. Subsequently, excess TAT were removed by repeatedly washing the nanoparticles with 0.1x PBS several times. Finally, MSN-$PEG_{3.4k}$-Ab-TAT were dispersed in 0.1x PBS and stored at 4 °C.

Fluorescence spectrometric determination of NF-κB p65 antibody conjugated onto MSN-$PEG_{3.4k}$-Ab(1:24)-TAT.

This journal is © The Royal Society of Chemistry 2012

To calibrate the amount of NF-κB p65 antibody on MSN, rhodamine B isothiocyanate (RITC) labeled p65 antibody was prepared. 2 mg of p65 antibody was dissolved in 0.1 M sodium bicarbonate solution (pH 9) at a concentration of 1 mg/mL. Then, 2.4 mg of RITC (prepared in 100 μL dimethyl sulfoxide) was added to the p65 antibody solution. After stirring for 12 h at 4℃, the unreacted RITC was removed by dialysis. RITC-p65 antibody was added to react with non-FITC MSN-$PEG_{3.4k}$-MAL to yield MSN-$PEG_{3.4k}$-RITC-Ab(1:24). About 0.1-0.2 mg of MSN-$PEG_{3.4k}$-RITC-Ab (1:24) was dissolved in 1 mL NaOH (1N) and centrifuged. The supernatant sample was read using HITACHI fluorescence spectrometer F-4500 (excited at 543 nm / emitted at 575 nm). The amount of RITC-p65 antibody on MSN-$PEG_{3.4k}$-RITC-Ab(1:24) was read out from a calibration curve established by plotting the fluorescence verses the concentration of free RITC- p65 antibodies in 1N NaOH.

Fluorescence spectrometric determination of TAT peptide conjugated onto MSN-PEG3.4k-Ab(1:24)-TAT.

Rhodamine B isothiocyanate (RITC) labeled Cys-TAT peptide (RITC-TAT) was conjugated with non-FITC MSN-$PEG_{3.4k}$-Ab(1:24) in 0.1x PBS solution to yield MSN-$PEG_{3.4k}$-Ab(1:24)-RITC-TAT. After conjugation, MSN-$PEG_{3.4k}$-Ab(1:24)-RITC-TAT was dissolved in 1 mL NaOH (1N) and the supernatant was collected after centrifugation. The RITC fluorescence of the supernatant was read using HITACHI fluorescence spectrometer F-4500 (excited at 543 nm / emitted at 575 nm). Finally, the concentration of the RITC-TAT peptide in the supernatant was determined according to the calibration curve established by plotting the fluorescence verses the concentration of free RITC-TAT peptide in 1N NaOH. The amount of TAT peptide conjugated onto the MSN-$PEG_{3.4k}$-Ab(1:24)-TAT was derived from the total supernatant peptide minus nanoparticle after conjugation.

Western blotting analysis.

Cell lysates were separated on a 10% SDS-PAGE, and the proteins were then electrophoretically transferred to a polyvinylidene difluoride (PVDF) membrane and blocked 1 h at room temperature in blocking buffer [1xTris-buffered saline (TBS)-0.1% Tween 20, 5% w/v nonfat dry milk]. Membranes were incubated overnight at 4 °C with primary antibodies : NF-κB p65, TNF-α , Lamin B and GAPDH from Santa Cruz Biotechnology (Santa Cruz, CA), along with COX-2 from Cayman (Cayman, Ann Arbor, MI, USA). All primary antibodies were diluted in blocking buffer (NF-κB p65: 1:500, TNF-α: 1:500, Lamin B: 1:3500, GAPDH: 1:5000 and COX-2: 1:500 dilution). The PVDF membranes were extensively washed and incubated with a horseradish peroxidase–conjugated secondary immunoglobulin G antibody (1: 2000 dilution, Santa Cruz Biotechnology) for 1 h at room temperature. Immunoreactive bands were visualized with an enhanced chemiluminescence substrate kit (Amersham Pharmacia Biotech, GE Healthcare UK Ltd, Bucks, UK) according to the manufacturer's protocol.

Cellular response of NF-κB on MSN-PEGs and *in vitro* pull-down assay of MSN-$PEG_{3.4k}$-Ab-TAT.

100 μg/mL of MSN-APTMS, MSN-PEG_{2k} and MSN-$PEG_{3.4k}$ were treated in HeLa cells for 4 h, and then incubation without or with TNF-α (50 ng/mL), a NF-κB activator, for another 0.5 h. After the cells were harvested, cytosolic and nuclear protein were isolated, the p65 expression level in either cytosol or nucleus was determined by western blotting experiment. For *in vitro* pull-down assay, the MSN-$PEG_{3.4k}$-Ab-TAT (100 μg/mL) was mixed and incubated with total lysate of HeLa cell at 4 °C for 18 h *in vitro*. Then, the mixture was centrifuged at 12,000 rpm for 20 min and the supernatant (10 μL) was assayed for the free p65 expression level by Western blotting.

Immunocytochemical staining for NF-κB p65 or Nup 153 expression.

HeLa cells were fixed with 4% paraformaldehyde and permeabilized with 0.1% Triton X-100. After being washed in PBS, cells were blocked in blocking buffer [1xTris-buffered saline (TBS)-0.1% Tween 20, 5% w/v BSA] for 1 h and then incubated with a NF-κB p65 (1:50 dilution, Santa Cruz Biotechnology) or Nup 153 (1:100 dilution, Abcam) primary antibody in blocking buffer for 16 h at 4 °C. The cells were extensively washed and incubated with Alexa-568 fluorescein-labeled secondary antibody in blocking buffer at a dilution of 1/200 for 2 h, and counterstained for nuclei with DAPI (DNA marker) for 1 min. The fluorescent images were obtained with a confocal laser scanning microscope (TCS SP5, Leica). For further images analysis of Figure 4b, the distribution map of distance between nanoparticles and nuclear membrane were calculated by MetaMorph software and Matlab program. The central point of cell nuclear and the mean radius of nuclear membrane of each cell, which were shown as the figure 4b with original point and dash line, were estimated by MetaMorph. Then, the fluorescence intensity of the nanoparticles with a distance relative to the nuclear membrane was summated to plot the distribution map by Matlab program.

Determination of nuclear NF-κB activation by ELISA.

The nuclear extracts and NF-κB activity were performed according to the manufacturer's protocol (NF-κB/p65 ActivELISA™ kit, Imgenex, San Diego, CA). The optical density of samples was determined by using the ELISA reader set at 405 nm.

Acknowledgements

This research was supported by National Taiwan University and the Ministry of Science and Technology (MOST) of Taiwan. We thank Ms. Hui-Min Chen (Taipei Medical University, Taiwan) for assistance in Bio-TEM experiments, and Mr. Shih-Hsin Huang for help in the sketching of nanoparticle schematic diagram.

Notes and references

[r] Department of Chemistry, National Taiwan University, Taipei 106, Taiwan

[f] Research Center of Applied Science, Academia Sinica, Taipei 115, Taiwan
[g] Department of Biochemistry and Molecular Cell Biology, Taipei Medical University, Taipei 110, Taiwan
[h] Department of Optics and Photonics, National Central University, Chung-Li 320, Taiwan

Electronic Supplementary Information (ESI) available: Detailed experimental procedures, nitrogen adsorption and desorption isotherms, powder X-ray diffraction (XRD), FT-IR, TEM, dynamic light scattering (DLS), zeta potential and cell experiments. See DOI: 10.1039/b000000x/

1. A. Kaffman and E. K. O'Shea, Annu. Rev. Cell Dev. Biol., 1999, 15, 291-339.
2. H. M. Johnson, P. S. Subramaniam, S. Olsnes and D. A. Jans, BioEssays, 2004, 26, 993-1004.
3. M. S. Cyert, J. Biol. Chem., 2001, 276, 20805-20808.
4. P. Brennan, R. Donev and S. Hewamana, Mol. BioSyst., 2008, 4, 909-919.
5. M. D. Shoulders, L. M. Ryno, C. B. Cooley, J. W. Kelly and R. L. Wiseman, J. Am. Chem. Soc., 2013, 135, 8129-8132.
6. W. Xu, M. R. Edwards, D. M. Borek, A. R. Feagins, A. Mittal, J. B. Alinger, K. N. Berry, B. Yen, J. Hamilton, T. J. Brett, R. V. Pappu, D. W. Leung, C. F. Basler and G. K. Amarasinghe, Cell Host Microbe, 2014, 16, 187-200.
7. D. Jurk, C. Wilson, J. F. Passos, F. Oakley, C. Correia-Melo, L. Greaves, G. Saretzki, C. Fox, C. Lawless, R. Anderson, G. Hewitt, S. L. Pender, N. Fullard, G. Nelson, J. Mann, B. van de Sluis, D. A. Mann and T. von Zglinicki, Nat. Commun., 2014, 2, 4172.
8. S. C. Gupta, C. Sundaram, S. Reuter and B. B. Aggarwal, Biochim. Biophys. Acta, 2010, 1799, 775-787.
9. Y. Kabe, K. Ando, S. Hirao, M. Yoshida and H. Handa, Antioxid. Redox Signaling, 2005, 7, 395-403.
10. M. Karin, Y. Cao, F. R. Greten and Z. W. Li, Nat. Rev. Cancer, 2002, 2, 301-310.
11. K. S. Ahn and B. B. Aggarwal, Ann. N. Y. Acad. Sci., 2005, 1056, 218-233.
12. E. Pikarsky, R. M. Porat, I. Stein, R. Abramovitch, S. Amit, S. Kasem, E. Gutkovich-Pyest, S. Urieli-Shoval, E. Galun and Y. Ben-Neriah, Nature, 2004, 431, 461-466.
13. M. Karin and F. R. Greten, Nat. Rev. Immunol., 2005, 5, 749-759.
14. F. R. Greten and M. Karin, Cancer Lett., 2004, 206, 193-199.
15. C. H. Lee, Y. T. Jeon, S. H. Kim and Y. S. Song, BioFactors, 2007, 29, 19-35.
16. H. M. Yang, C. W. Park, M. A. Woo, M. I. Kim, Y. M. Jo, H. G. Park and J. D. Kim, Biomacromolecules, 2010, 11, 2866-2872.
17. P. A. McCarron, W. M. Marouf, D. J. Quinn, F. Fay, R. E. Burden, S. A. Olwill and C. J. Scott, Bioconjugate Chem., 2008, 19, 1561-1569.
18. M. Rizzuti, M. Nizzardo, C. Zanetta, A. Ramirez and S. Corti, Drug Discovery Today, 2015, 20, 76-85.
19. F. Lu, S. H. Wu, Y. Hung and C. Y. Mou, Small, 2009, 5, 1408-1413.
20. S. H. Wu, C. Y. Mou and H. P. Lin, Chem. Soc. Rev., 2013, 42, 3862-3875.
21. Y. P. Chen, C. T. Chen, Y. Hung, C. M. Chou, T. P. Liu, M. R. Liang, C. T. Chen and C. Y. Mou, J. Am. Chem. Soc., 2013, 135, 1516-1523.
22. C. H. Wu, Y. P. Chen, C. Y. Mou and R. P. Cheng, Amino acids, 2013, 44, 473-480.
23. L. Pan, J. Liu, Q. He and J. Shi, Adv. Mater., 2014, 26, 6742-6748.
24. L. Pan, Q. He, J. Liu, Y. Chen, M. Ma, L. Zhang and J. Shi, J. Am. Chem. Soc., 2012, 134, 5722-5725.
25. L. Pan, J. Liu, Q. He, L. Wang and J. Shi, Biomaterials, 2013, 34, 2719-2730.
26. R. J. Anto, A. Mukhopadhyay, S. Shishodia, C. G. Gairola and B. B. Aggarwal, Carcinogenesis, 2002, 23, 1511-1518.
27. A. C. Bharti and B. B. Aggarwal, Biochem. Pharmacol., 2002, 64, 883-888.
28. A. Richmond, Nature Reviews Immunology 2002, 2, 664-674.
29. D. C. Duffey, Z. Chen, G. Dong, F. G. Ondrey, J. S. Wolf, K. Brown, U. Siebenlist and C. Van Waes, Cancer Res., 1999, 59, 3468-3474.
30. D. C. Duffey, C. V. Crowl-Bancroft, Z. Chen, F. G. Ondrey, M. Nejad-Sattari, G. Dong and C. Van Waes, Br. J. Cancer, 2000, 83, 1367-1374.
31. D. G. Jackson-Bernitsas, H. Ichikawa, Y. Takada, J. N. Myers, X. L. Lin, B. G. Darnay, M. M. Chaturvedi and B. B. Aggarwal, Oncogene, 2007, 26, 1385-1397.
32. L. Schermelleh, P. M. Carlton, S. Haase, L. Shao, L. Winoto, P. Kner, B. Burke, M. C. Cardoso, D. A. Agard, M. G. Gustafsson, H. Leonhardt and J. W. Sedat, Science, 2008, 320, 1332-1336.
33. A. Efthymiadis, L. J. Briggs and D. A. Jans, J. Biol. Chem., 1998, 273, 1623-1628.
34. F. Cardarelli, M. Serresi, A. Albanese, R. Bizzarri and F. Beltram, J. Biol. Chem., 2011, 286, 12292-12299.
35. Y. S. Lin, N. Abadeer, K. R. Hurley and C. L. Haynes, J. Am. Chem. Soc., 2011, 133, 20444-20457.
36. Y. S. Lin, N. Abadeer and C. L. Haynes, Chem. Commun., 2011, 47, 532-534.
37. O. Cohen and R. Granek, Nano Lett., 2014, 14, 2515-2521.
38. C. H. Wu, Y. P. Chen, S. H. Wu, Y. Hung, C. Y. Mou and R. P. Cheng, ACS Appl. Mater. Interfaces, 2013, 5, 12244-12248.
39. Y. S. Lin, C. P. Tsai, H. Y. Huang, C. T. Kuo, Y. Hung, D. M. Huang, Y. C. Chen and C. Y. Mou, Chem. Mater., 2005, 17, 4570-4573.

This journal is © The Royal Society of Chemistry 2012

small
NANO MICRO

Intracellular Implantation of Enzymes in Hollow Silica Nanospheres for Protein Therapy: Cascade System of Superoxide Dismutase and Catalase

*Feng-Peng Chang, Yi-Ping Chen, and Chung-Yuan Mou**

An approach for enzyme therapeutics is elaborated with cell-implanted nanoreactors that are based on multiple enzymes encapsulated in hollow silica nanospheres (HSNs). The synthesis of HSNs is carried out by silica sol–gel templating of water-in-oil microemulsions so that polyethyleneimine (PEI) modified enzymes in aqueous phase are encapsulated inside the HSNs. PEI-grafted superoxide dismutase (PEI-SOD) and catalase (PEI-CAT) encapsulated in HSNs are prepared with quantitative control of the enzyme loadings. Excellent activities of superoxide dismutation by PEI-SOD@HSN are found and transformation of H_2O_2 to water by PEI-CAT@HSN. When PEI-SOD and PEI-CAT are co-encapsulated, cascade transformation of superoxide through hydrogen peroxide to water was facile. Substantial fractions of HSNs exhibit endosome escape to cytosol after their delivery to cells. The production of downstream reactive oxygen species (ROS) and COX-2/p-p38 expression show that co-encapsulated SOD/CAT inside the HSNs renders the highest cell protection against the toxicant N,N′-dimethyl-4,4′-bipyridinium dichloride (paraquat). The rapid cell uptake and strong detoxification effect on superoxide radicals by the SOD/CAT-encapsulated hollow mesoporous silica nanoparticles demonstrate the general concept of implanting catalytic nanoreactors in biological cells with designed functions.

1. Introduction

In biological cells, a great variety of enzymatic catalysis is responsible for energy conversion, synthesis, and cellular defense to maintain physiological functionality. To tightly regulate multiple reactive species in the crowded cellular environment, compartmentalization is a dominant feature in eukaryotic cells. This is to keep enzymes and biomolecules together to reach a higher concentration and to lead to orderly control of complex cascade reactions. Cascade enzymatic reactions of the glyoxylate cycle, Calvin cycle, and Krebs cycle in an organelle enclosure are examples of catalyzed reactions by confined enzymes.

Inspired by the compartmentalized structure in living cells, building hollow porous nanostructured materials to encapsulate multiple enzymes would be a very promising approach in biomedicine for enhancing, repairing, or adding new functionalities to cells.[1] Such strategy of synthetic organelles implanted into cells is still at its nascent stage of development.[2] Tandem enzyme reactions are mostly demonstrated in test tubes using liposomes,[3] polymer-based materials,[4–11] or gelatin microcapsules.[12] The challenges of existing materials are overcoming poor stability, their micrometer-size range, their slow cell uptake, and low permeability toward small molecules that hampers their function as organelle-mimics in cells.

Recently, we reported a microemulsion-template method[9] for synthesizing hollow silica nanospheres (HSNs), with large interior spaces and porous silica shells, suitable

F.-P. Chang, Prof. C.-Y. Mou
Department of Chemistry
National Taiwan University
Taipei 106, Taiwan
E-mail: cymou@ntu.edu.tw
Dr. Y.-P. Chen
Research Center for Applied Sciences Academia Sinica
Taipei 115, Taiwan

DOI: 10.1002/smll.201401559

© 2014 Wiley-VCH Verlag GmbH & Co. KGaA, Weinheim

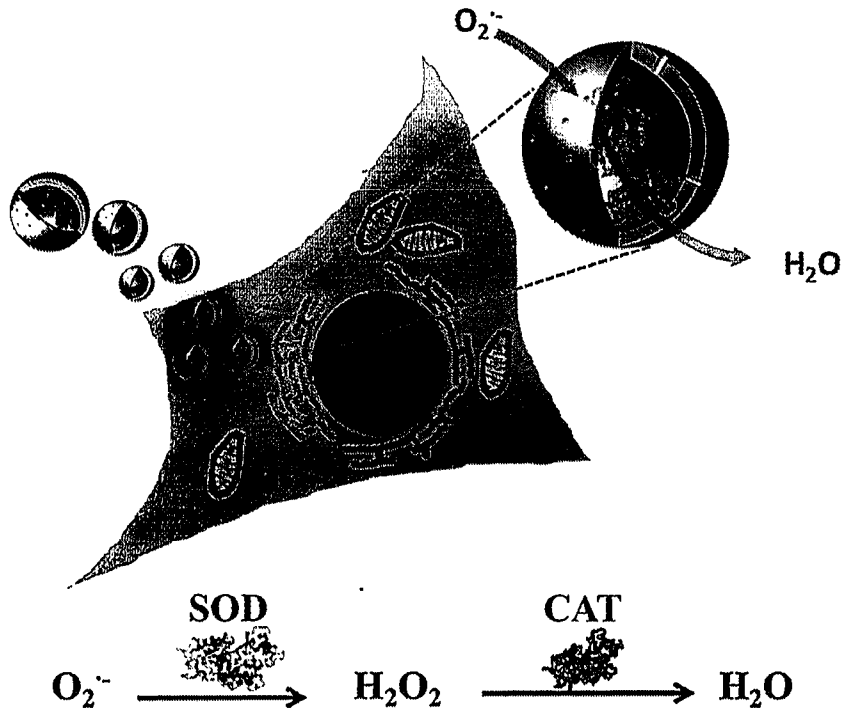

Scheme 1. Schematic representation of the cascade reaction of superoxide dismutase and catalase encapsulated HSNs acting inside cells.

for loading enzymes in the cavity to carry out intracellular catalysis. We demonstrated encapsulation of horseradish peroxidase (HRP) in the cavity of HSNs and its intracellular delivery showing its function as a catalytic nanoreactor inside Hela cells for converting a pro-drug into a toxic agent that killed cancer cells.[13] For biomedical applications, HSNs possess several key properties as an intracellular nanoreactor: 1) a porous shell with permeability for small molecules, subtracts, and products,[18] while protecting enzymes against poison,[14] protease,[13] and attenuated immunological responses, 2) a properly designed size and a surface ligand so that the nanoparticles can be taken up by targeted cells,[15,16] 3) a good stability and biocompatibility,[17] and 4) multi-functional capability such as pH sensing,[19,20] MRI for tracking,[21] or synergistic therapy for cancer treatment.[22–25]

The next development would be a functional multiple-enzyme assembly encapsulated in porous HSNs such that cascade reactions can be realized. We chose to study a superoxide dismutase (SOD)/catalase (CAT) system for detoxification of reactive oxygen species (ROS); SOD converts superoxide into hydrogen peroxide, which is, in turn, transformed to water and oxygen by catalase. SOD has the highest catalytic efficiency (k_{CAT}/K_m) whereas CAT has a turnover of 40 million molecules of H_2O_2 degraded per second.[26] Therefore, the enzymatic antioxidant intervention offers superior efficacy for ROS quenching not attainable by small-molecule antioxidants.[27] A significant hurdle in the translation of the antioxidant enzyme strategy into the clinical domain lies in the inadequate delivery of multiple enzymes into the intended cells while keeping them functioning together. At present, the only reported nanocarrier for cell delivery of multiple enzymes is using polymeric vesicles. Tanner et al. have demonstrated that a coupled superoxide dismutase/lactoperoxidase enzyme system working within triblock copolymers vesicles could serve as artificial peroxisomes to protect cells from ROS stress.[7,28] However, their biocompability, slow cell uptake, and poor material transport across the polymeric membrane remained problematic.

In contrast, as discussed above, hollow silica nanospheres offer many design capabilities and better biocompability.[22,29] In this paper, we report a cascade-reaction system in hollow silica nanospheres, where polyethyleneimine (PEI)-grafted superoxide dismutase (PEI-SOD) and catalase (PEI-CAT) were co-encapsulated in the cavity of substrate-permeable HSNs (named PEI-SOD/CAT@HSN). The cationic PEI serves several functions: 1) increasing the loading efficiency of SOD and CAT in the HSNs; 2) augmenting the proton sponge effect for endosome escape into the cytoplasm; and 3) the positively charged PEI helps to attract the counter-charged superoxide anion into diffusing into the HSNs. After introduction into the cells, the organelle-mimic PEI-SOD/CAT@HSN is shown to detoxify ROS, superoxide, and hydrogen peroxide successively and protect the cells. **Scheme 1** illustrates the peroxisome-like PEI- SOD/CAT@HSN inside the cell for ROS detoxification. We demonstrate the synergy effects of SOD and CAT in the HSN cavity.

With further surface functionalization for targeting this approach could result in a carefully designed nanosystem of encapsulated enzymes mimicking intracellular organelles for therapeutic purposes.

2. Results and Discussion

2.1. Synthesis of Enzyme-Encapsulated Nanospheres

Previously, we developed a one-pot method to encapsulate horseradish peroxidase (HRP) in HSNs, which activated indole-3-acetic acid intracellularly for cancer therapy.[13] Based on the previous method, we introduced PEI in this system to improve the enzyme loading. PEI, with its rich amine groups, has been demonstrated to be good proton sponge for the endosome-escape effect.[30,31] PEI by itself disrupts cell membranes and mitochondria and is, thus, very cytotoxic.[32,33] Herein, we report a novel strategy whereby PEI-grafted enzymes were encapsulated inside HSNs. The silica shell shields off the PEI from contacting the cellular machinery while still keeping the proton-sponge effect of PEI as the pores on the shell do allow protons to diffuse inside the hollow spheres.

Scheme 2 illustrates the preparation for PEI-modification and then the encapsulation of the positively charged PEI-SOD and PEI-CAT in HSNs. Both SOD and CAT

 © 2014 Wiley-VCH Verlag GmbH & Co. KGaA, Weinheim

NANO MICRO small

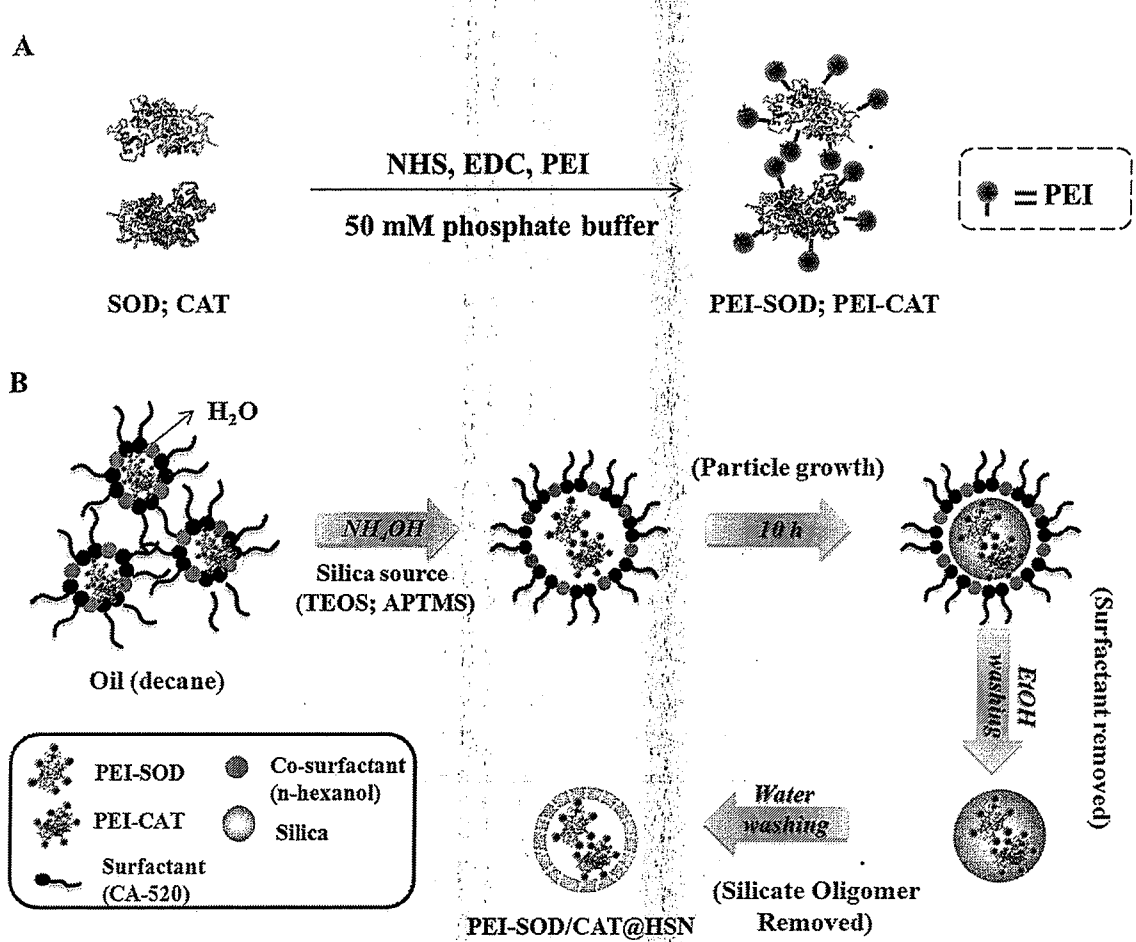

Scheme 2. Preparation and encapsulation of PEI-enzymes. A)Scheme of PEI-enzyme conjugation by amidation of the carboxyl group with PEI. B) Schematic illustration for the synthesis of PEI-SOD and PEI-CAT co-encapsulated hollow silica nanospheres (PEI-SOD/CAT@HSN).

are important antioxidant enzymes in living systems. As depicted in Scheme 2A, PEI was covalently linked to the enzymes by a conventional ethyl(dimethylaminopropyl) carbodiimide/*N*-hydroxysuccinimide (EDC/NHS) coupling reaction. Subsequently, PEI-grafted enzymes, PEI-SOD, PEI-CAT, either single or together, were encapsulated in the HSNs by a one-pot water-in-oil (w/o) microemulsion silica templating approach (Scheme 2B). In brief, an aqueous solution containing the PEI-grafted enzymes was emulsified in an oil system containing a surfactant (isooctylphenyl ether, CA-520), co-surfactant (*n*-hexanol), and organic solvent (decane). After introducing the silica sources (tetraethoxysilane (TEOS) and aminopropyltrimethoxy silane (APTMS)) and aqueous ammonia the w/o mixture was stirred for 10 h at 20 °C to form the enzyme-encapsulated silica nanoparticles. Hollow enzyme-loaded particles were formed after the nanoparticles were further suspended in warm deionized water (40 °C) for 40 min and washed with water, which is critical for the transformation to hollow nanospheres.

2.2. Physicochemical Characterization

The surface area of our HSNs (231.2 $m^2 g^{-1}$) as determined by N_2 adsorption–desorption isotherms exhibited characteristic type-IV Brunauer–Emmett–Teller (BET) isotherms (Figure S1, Supporting Information). The high surface area can be attributed to the porous structure on the shell, indicating that most of the surfactants have been removed. **Figure 1**A shows transmission electron microscopy (TEM) images of PEI-SOD/CAT@HSN (Figure S2 in the Supporting Information shows the TEM images of PEI-SOD@HSN and PEI-CAT@HSN). All particles show a narrow size distribution, with an average diameter of around 40 nm. Uranyl acetate (UA) staining displayed an enhanced electron density inside the PEI-SOD/CAT@HSN particles but no staining outside the particles (Figure 1B). This indicates that the enzymes were indeed entrapped within the hollow spheres. To examine the enzyme-encapsulation efficiency and loading yields, fluorescent dye-labeled enzymes (rhodamine B isothiocyanate (RITC) and fluorescein isothiocyanate (FITC)) were prepared. SOD and PEI-SOD were labeled with FITC and abbreviated as FITC-SOD and FITC-PEI-SOD. CAT and PEI-CAT were marked with RITC and abbreviated as RITC-CAT and RITC-PEI-CAT. The fluorescence intensity of the dye-enzyme-loaded HSNs were measured by suspending the nanoparticles in 1N NaOH and the amount of encapsulated dye enzymes was determined from the calibration curve established by plotting the fluorescence versus the concentration of free dye enzymes under the same conditions (Figure S3 in the Supporting Information shows the calculation of both PEI-SOD and PEI-CAT inside PEI-SOD/CAT@HSN).[13] Significantly

© 2014 Wiley-VCH Verlag GmbH & Co. KGaA, Weinheim

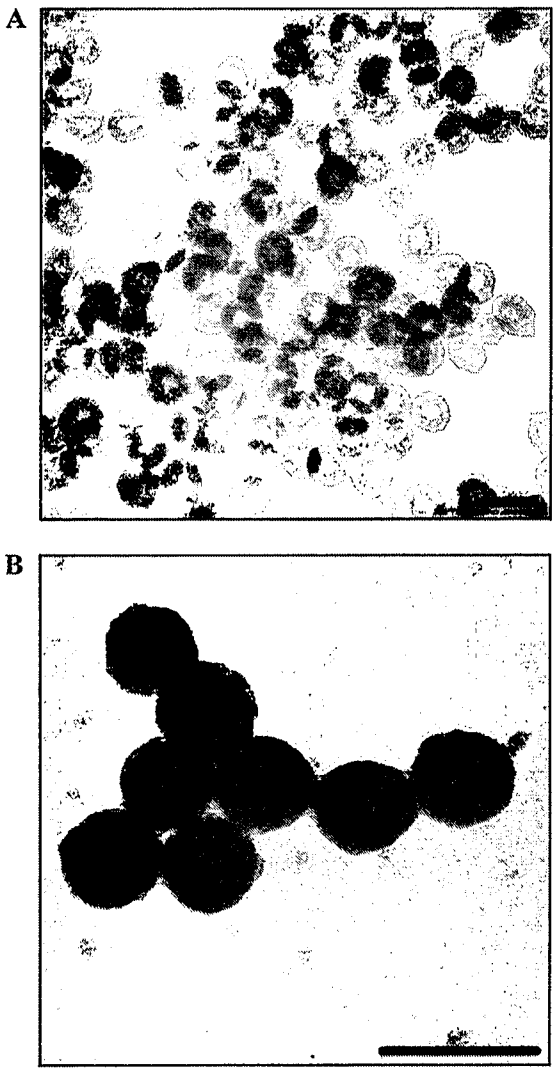

Figure 1. TEM images of A) PEI-SOD/CAT@HSN, B) PEI-SOD/CAT@HSN stained with uranyl acetate (UA). UA-staining showed the enhanced electron density in the cavity of the HSNs. The scale bars are 100 nm for both images.

higher amounts of enzymes were encapsulated in the HSNs in the presence of the cationic polymer PEI (Table S1, Supporting Information). The loading efficiencies of PEI-SOD (12.2%) and PEI-CAT (8.7%) were much higher than that of SOD (2.8%) and CAT (2.8%). This is related to the fact that the positively charged PEI-SOD and PEI-CAT (Figure S4, Supporting Information) are more effective in attracting the negatively charged hydrolyzed silica precursors for encapsulation. The higher loading will improve the enzyme activity for biomedical uses and thus we chose the PEI-coated enzymes for further study. The loading yields of the PEI-SOD@HSN and PEI-CAT@HSN particles were 44.7 and 29.5 μg enzymes per mg HSNs, respectively. Compared to single-enzyme loading, about the same level of efficiency and loading yields were observed when two enzymes, PEI-SOD and PEI-CAT, were co-encapsulated in HSNs. The loading efficiency of PEI-SOD and PEI-CAT were 12.3% and 9.4%, respectively. PEI-SOD/CAT@HSN contained about 44.5 and 26.1 μg enzymes per mg HSNs (Table S1, Supporting Information).

We also characterized the suspension of the nanoparticles in deionized water and in Dulbecco's modified Eagle's medium (DMEM), which is a cell culture medium. Dynamic light scattering (DLS) (Table S2, Supporting Information) showed that the hydrodynamic sizes of PEI-SOD/CAT@HSN and HSNs were 130.7 (±0.9) and 176.8 (±0.8) nm, respectively. It was seen that serious aggregation occurred upon dispersion in DMEM. In order to improve the dispersion of the nanoparticles in cell-culture medium, we stabilized the nanoparticles with bovine serum albumin (BSA)[34] after which the DLS size of PEI-SOD/CAT@HSN and HSNs in DMEM decreased from 973.8 nm (±127.2) and 1271.3 (±204.4) (without BSA) to 221.7 nm (±30.3) and 302.8 (±24.0) (with BSA), respectively. Because of the cationic property of PEI, the zeta potential of PEI-SOD/CAT@HSN was higher than that of HSNs in the mediums of H_2O, DMEM, and BSA-stabilized in DMEM.

2.3. Activity of Encapsulated SOD

In order to measure the SOD activity, we used xanthine/xanthine oxidase as the superoxide anion ($O_2^{\bullet-}$) generator and detected the capacity of PEI-SOD/CAT@HSN for inhibiting the rate of reduction of cytochrome c by superoxide (**Figure 2**A). In the absence of SOD, $O_2^{\bullet-}$ reduces cytochrome c to form a yellow product (absorption at 550 nm). In the presence of SOD, the concentration of superoxide is reduced, yielding a less colored signal. The calibration curve for native SOD inhibition is given in Figure S5 in the Supporting Information. Figure 2A showed that the increase in absorption can clearly be observed according to the reaction time in the blank (control; SOD-free) and the reaction rate was unaffected by HSNs and PEI-CAT@HSN (negative control). However, in the presence of PEI-SOD@HSN and PEI-SOD/CAT@HSN, the kinetics of $O_2^{\bullet-}$ consumption increased and the reduction rate of cytochrome c was significantly inhibited. It is worthwhile notign that the SOD activity of PEI-SOD/CAT@HSN is higher than that of PEI-SOD@HSN although equal doses of SOD were employed in both particles. We suggest that for the PEI-SOD@HSN an inactivation of SOD occurred because of the large excesses of H_2O_2 generated by SOD and the $O_2^{\bullet-}$ existing in the PEI-SOD@HSN solution. This inhibition effect has been attributed to the reduction of enzyme-bound Cu^{2+} to Cu^{1+} by H_2O_2.[35] However, in the presence of CAT, the hydrogen peroxide was removed quickly and thus PEI-SOD/CAT@HSN maintained its high SOD activity. Comparing the inhibition percentage of cytochrome c reduction between native SOD (Figure S5, Supporting Information) and SOD-loaded particles, the encapsulated PEI-SOD/CAT@HSN and PEI-SOD@HSN maintained 46.6% and 18.6% of the native SOD activity (Table S3, Supporting Information).

2.4. Activity of Encapsulated CAT

CAT catalyzes the decomposition of hydrogen peroxide into water and oxygen. To detect the catalase activity, we directly measured the degradation of H_2O_2 using a horseradish

 © 2014 Wiley-VCH Verlag GmbH & Co. KGaA, Weinheim

NANO MICRO small

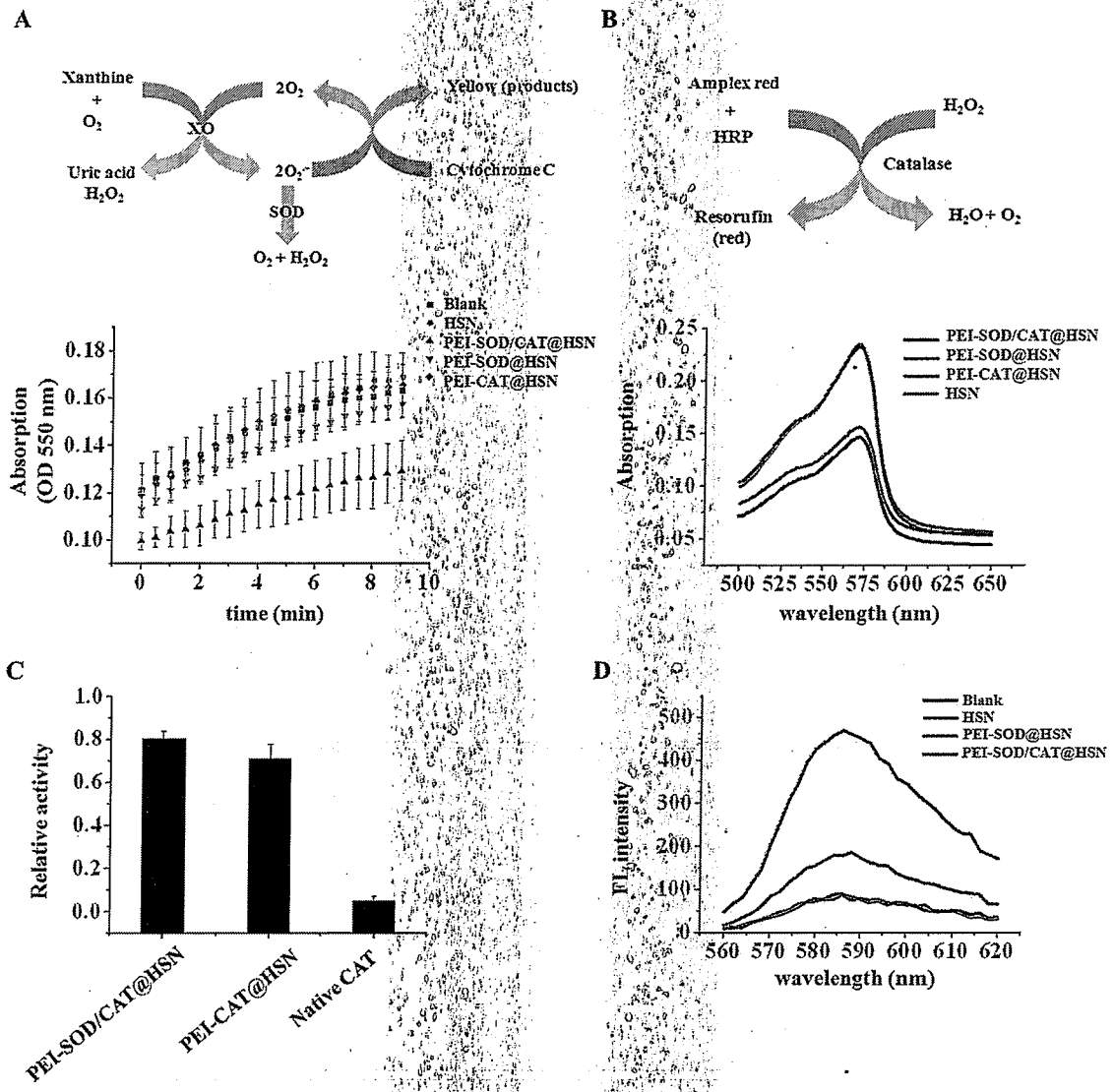

Figure 2. Enzyme activity assay. A) Superoxide anions, ($O_2^{\bullet-}$) are generated by a xanthin/xanthine oxidase system and then detected with cytochrome c. The reduction kinetics of cytochrom c were assayed in the presence of various samples. B) CAT activity assayed using a horseradish peroxidase (HRP)/Amplex-red system to measure the H_2O_2 degradation. The UV-vis spectra of various samples were measured after incubation with H_2O_2 and then assayed with HRP/Amplex red. C) Stability of CAT-loaded particles and native CAT after treatment with KO_2 solution. The relative enzyme activity is expressed as the ratio of change in absorption at 570 nm before and after KO_2 treatment. D) Cascade reactions within PEI-SOD/CAT@HSN. The fluorescence intensity reflects the amount of H_2O_2 in the assay buffer. Here the same amount of SOD units in PEI-SOD/CAT@HSN and PEI-SOD@HSN were used for comparison.

peroxidase/Amplex-red method (Figure 2B).[36] In the presence of peroxidase, the Amplex-red reagent reacts with H_2O_2 to produce the red-colored oxidation product, resorufin. The change in absorption at 570 nm is proportional to the catalase activity. The results in Figure 2B show that PEI-SOD/CAT@HSN and PEI-CAT@HSN significantly decreased the amount of H_2O_2 compared to HSNs and PEI-SOD@HSN (negative control), demonstrating that H_2O_2 was indeed reduced by catalase. Comparing the reaction rate of H_2O_2 decomposition between native CAT (Figure S6, Supporting Information) and CAT-loaded particles, it cna be seen that PEI-SOD/CAT@HSN and CAT@HSN retained 57.9% and 62.7% of the native CAT activity (Table S3, Supporting Information).

We next explored the synergism between SOD and CAT in the presence of $O_2^{\bullet-}$. As shown in Figure 2C, after exposure to KO_2 solution, which generates $O_2^{\bullet-}$,[37] native CAT lost almost all its activity, whereas the CAT activity of PEI-SOD/CAT@HSN and PEI-CAT@HSN remained at about 80% and 70%. The suppression of CAT activity by $O_2^{\bullet-}$ may be due to the conversion of CAT to the ferroxy state or ferryl state that was rapidly reversed by SOD.[38] However, the anti-superoxide radical effect of CAT not only existed in PEI-SOD/CAT@HSN but could also be found in the PEI-CAT@HSN. We need more studies to explain this phenomenon but it implies that encapsulated PEI-CAT will resist deactivation as well as protect SOD from H_2O_2 attack in the confined PEI-SOD/CAT@HSN.

2.5. Cascade Reactions in PEI-SOD/CAT@HSN

SOD and CAT are both antioxidant enzymes that can work together as primary defense system against free-radical

© 2014 Wiley-VCH Verlag GmbH & Co. KGaA, Weinheim

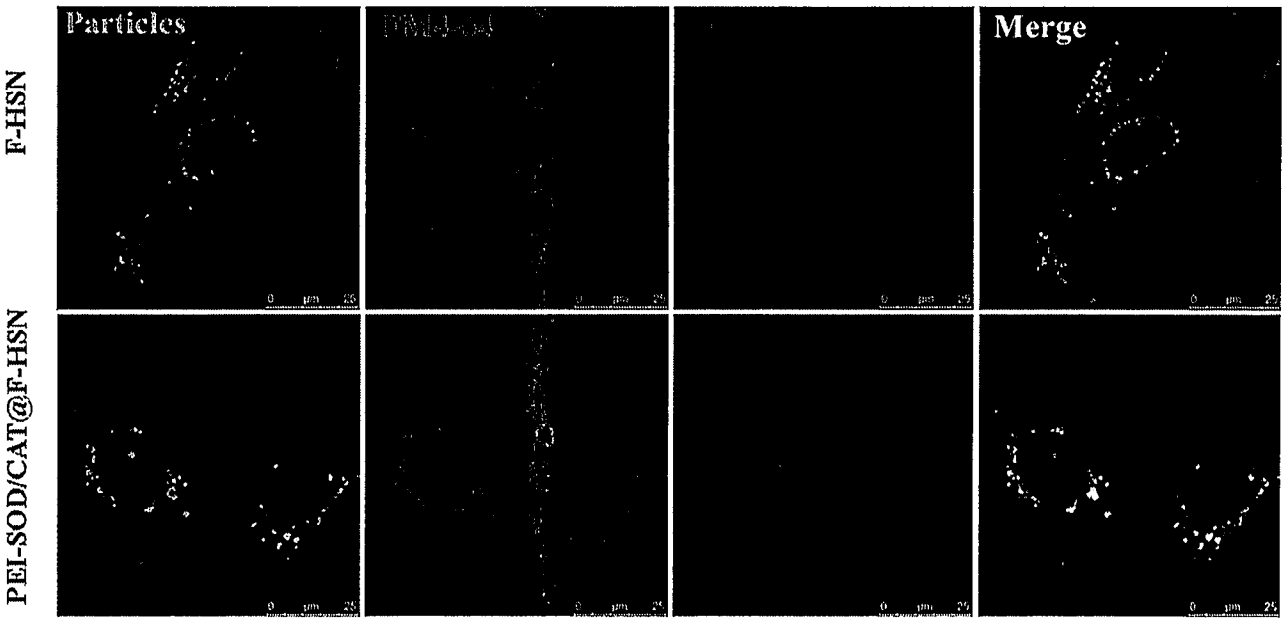

Figure 3. Confocal microscopy analysis of F-HSN and PEI-SOD/CAT@F-HSN in HeLa cells. Particle-treated cells were stained with endosome-specific marker FM4–64 (red) and analyzed for endosomal co-localization. Blue: DAPI-stained nuclei. Green signals in the merge channel indicate endosomal escape of the particles.

damage in living cells. In the study above, we have demonstrated that PEI-SOD and PEI-CAT can be simultaneously encapsulated in HSNs and the final nanoparticle system shows activities for both enzymes. In order to investigate whether both the encapsulated enzymes are involved in cascade reactions, fluorescence assay was performed in which the resorufin formation was recorded by monitoring the fluorescence at 570 nm (Figure S7, Supporting Information). In the reaction, the $O_2^{\bullet-}$ generated by KO_2 was unstable and converted to H_2O_2 in the presence or absence of SOD in aqueous solution. However, the dismutation rate of $O_2^{\bullet-}$ in the presence of SOD is faster. Subsequently, H_2O_2 could be either reduced by CAT or further involved in the peroxidase/Amplex-red oxidation reaction. As shown in Figure 2D, the fluorescence intensity of PEI-SOD@HSN was significantly higher than that of the blank (control), HSNs (negative control), and PEI-SOD/CAT@HSN systems. The results indicate that PEI-SOD@HSN catalyzed the reduction of $O_2^{\bullet-}$ to hydrogen peroxide and increases the rate of resorufin formation. However, in the presence of PEI-SOD/CAT@HSN cascade reactions occur. Hydrogen peroxide produced by SOD could be further decomposed by CAT and the system showed weaker fluorescence.

2.6. Cell Uptake, Distribution Pattern, and Cytotoxicity of PEI-Enzyme Loaded HSNs

To visualize the uptake distribution of BSA-stabilized nanoparticles, HSNs and PEI-SOD/CAT@HSN were doped with FITC (see experimental section) to form F-HSN and PEI-SOD/CAT@F-HSN. We treated HeLa cells with uptaken nanoparticles in the presence of the endosome marker (*N*-(3-triethylammoniumpropyl)-4-(4-diethylaminophenylhexatrienyl) pyridinium dibromide (FM4–64), red fluorescence). Confocal microscopy images (**Figure 3**) show that both kinds of nanoparticles (green channel) were well-internalized into the cells, in which little co-localization (yellow color) signals with FM4–64 stained organelles (red) were found. This indicates that most of the nanoparticles escaped from the endosome and resided in the cytoplasm (green dots in the merge channel). In our previous study, HRP-loaded HSNs (zeta potential = 20.5 mV) show proton-sponge effects due to the extensive amine groups in APTMS-doped silica shells.[13] Here HSNs and PEI-SOD/CAT@HSN with positive charges (40.1 mV and 25.4 mV, respectively, in H_2O) also showed similar intracellular patterns. We suggest that the carrier-only HSNs have some capability of endosome escape and the added PEI in PEI-enzyme@HSN further enhanced this effect. We next employed flow cytometry to quantify the cell uptake of the nanoparticles at the treated doses of 50, 100, and 200 μg mL^{-1} for 2.5 h. Remarkably high cellular uptakes of PEI- SOD/CAT@HSN (Figure S8, Supporting Information) were observed. The mean fluorescence intensity (calculated from Figure S8A) exhibited a dose-dependent uptake behavior of nanoparticles by HeLa cells (Figure S8C).

The issue of PEI's cytotoxicity is a concern when it is used as a cargo-carrier, as has been shown in previous reports.[32,33] To examine the toxic effect of PEI in our system, we used Western blotting assays to evaluate the PEI-induced p-p38 and COX2 expression. Both proteins are involved in inflammatory responses and reactive oxygen species (ROS)-related diseases.[39] HeLa cells were incubated with PEI-SOD, PEI-SOD@HSN, and HSNs for 2.5 h or further cultured in regular growth medium for 18 h. As shown in **Figure 4**A, the expressions of p-p38 for HSN-treated cells were at about the same level as in the control sample. We did find a little elevated expressions of p-p38 at 2.5 h after treatment with PEI-SOD and PEI-SOD@HSN. This is probably due to the stress of PEI-conjugated enzymes but it was repaired by the cells after

 © 2014 Wiley-VCH Verlag GmbH & Co. KGaA, Weinheim

NANO MICRO small

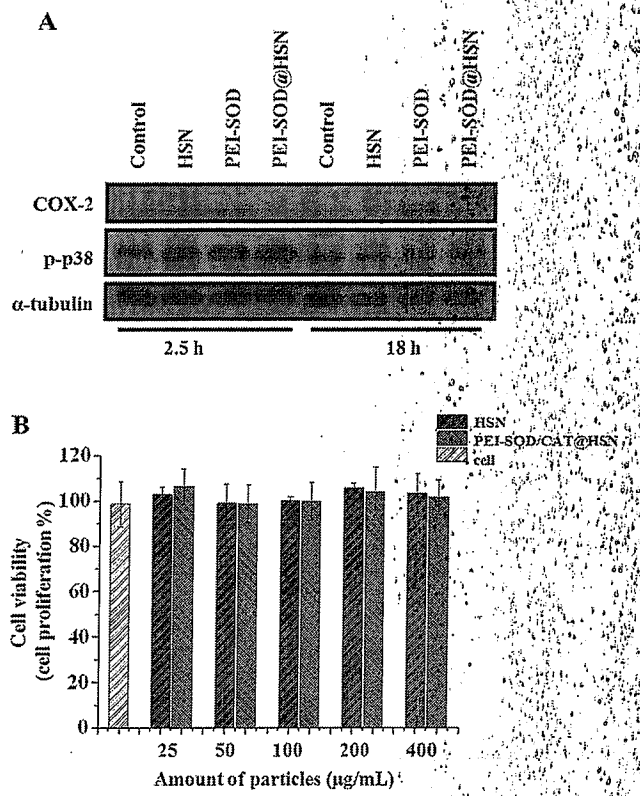

Figure 4. Western blotting and WST-1 assay to evaluate the cytotoxicity of PEI and enzyme-loaded particles. A) HeLa cells treated with PEI-SOD, HSNs, and PEI-SOD@HSN for 2.5 and 18 h. Here PEI-SOD and PEI-SOD/CAT@HSN have the same amount of enzymes. Particle doses were 100 μg mL^{-1}. Cellular levels of COX-2, p-p38, and α-tubulin were analyzed by Western blotting. α-tubulin was used as the loading control. B) Cells exposed to HSNs or PEI-SOD/CAT@HSN at doses of 25, 50, 100, 200, and 400 μg mL^{-1}. The cell viability was examined using WST-1 assay after 2.5 h of particle treatment followed by additional 24 h growth.

18 h of treatment. However, COX2, a downstream effector of p-p38, which plays a key role in the pathogenesis of inflammation, was up-expressed only in the case of PEI-SOD treatment. This shows that our strategy of encapsulating PEI-grafted enzymes within HSNs effectively shields the PEI's cytotoxicity. More importantly, no significant cytotoxicity of HSNs and PEI-SOD@HSN were found in cell proliferation assays even though the doses of the particles were as high as 400 μg mL^{-1} (Figure 4B). That no obvious cell cytotoxicity was observed after loading the nanoparticles also indicates that the toxic surfactants have been mostly removed and PEI has been well-shielded by the hollow nanospheres.

2.7. Protective Effect of Enzyme-Loaded Particles in Cells After Paraquat (PQ) Treatment

We have demonstrated that a tandem reaction occurs within PEI-SOD/CAT@HSN in test-tube experiments. The nanoparticles exhibited an excellent synergistic effect between SOD and CAT. They also displayed high bio-compatibility. These advantages may provide opportunities for their use in protein therapy. We therefore evaluated the capability of these enzyme-loaded particles in living cells for removing paraquat (PQ)-induced ROS.[40] HeLa cells were treated with various nanoparticles at a dose of 100 μg mL^{-1}. We measured the ROS production by flow cytometry with dihydroethidium (DHE), a superoxide indicator with fluorescence upon oxidation, to evaluate the antioxidant effect of each of the nanoparticles (**Figure 5**A). The PQ-induced ROS production was the same for the unprotected cells (positive control and HSNs only). As anticipated, all enzyme-nanoparticle treated cells obviously inhibited the PQ-induced ROS production. PEI-SOD@HSN and PEI-CAT@HSN showed a similar level of reduction of the DHE-positive cells by about 25% (compared to HSNs only). However, co-loaded PEI-SOD/CAT@HSN showed a much higher level of reduction of DHE-positive cells by about 60%. The PEI-SOD/CAT@HSN nanosystem clearly showed a synergistic effect for ROS reduction. We also measured the mean fluorescence intensity of PQ-treated cells. The ROS production for PEI-SOD/CAT@HSN also showed enhanced levels of reduction compared to PEI-SOD@HSN or PEI-CAT@HSN (Figure S9, Supporting Information). Quantitative analysis of the DHE-positive cells and fluorescence intensity indicated that PEI-SOD/CAT@HSN with its combination effect of both antioxidant enzymes displayed the weakest fluorescence intensity under microscopic observation (Figure 5B). Representative optical images (Figure S10, Supporitng Information) also show that the toxicity of PQ significantly changed the cell morphology (control +PQ and HSNs+PQ), which is consistent with previous reports.[41] However, the enzyme-loaded particles, especially PEI-SOD/CAT@HSN, showed a better attaching morphology as compared to the control+PQ. This also implies that the treatment with PEI-SOD/CAT@HSN detoxifies the imposed ROS. The nanoparticle-treated cells after incubation with PQ were further assayed with Western blotting to check the level of p-p38 and COX2 expression. Figure 5C clearly shows a down-regulation in the PQ-induced activation of p-p38 and COX2 when cells were pre-treated with PEI-SOD/CAT@HSN, PEI-SOD@HSN, and PEI-CAT@HSN. Furthermore, the levels of COX-2 show a much diminished expression for the PEI-SOD@HSN and PEI-CAT@HSN system to an almost unobservable level. It seems that the single-enzyme loaded particles are already enough to overcome the oxidative stress as expressed by the COX2 levels. The PEI-SOD/CAT@HSN particles hence show about the same level of COX2.

3. Conclusions

We have shown that it is possible to construct mesoporous hollow silica nanospheres (ca. 40 nm in size) based on a templating water-in-oil with sol-gel condensation. During the synthesis of the HSNs the enzymes SOD and/or catalase can be simultaneously or individually encapsulated within the HSNs with the help of PEI. The mesopores on the silica shell allow easy access of small molecules while keeping the enzymes inside the nanospheres to avoid undesirable protein–protein interactions. We found excellent catalytic activities of superoxide dismutation by SOD and subsequent transformation of H_2O_2 into water by CAT encapsulated in the HSNs. When

© 2014 Wiley-VCH Verlag GmbH & Co. KGaA, Weinheim

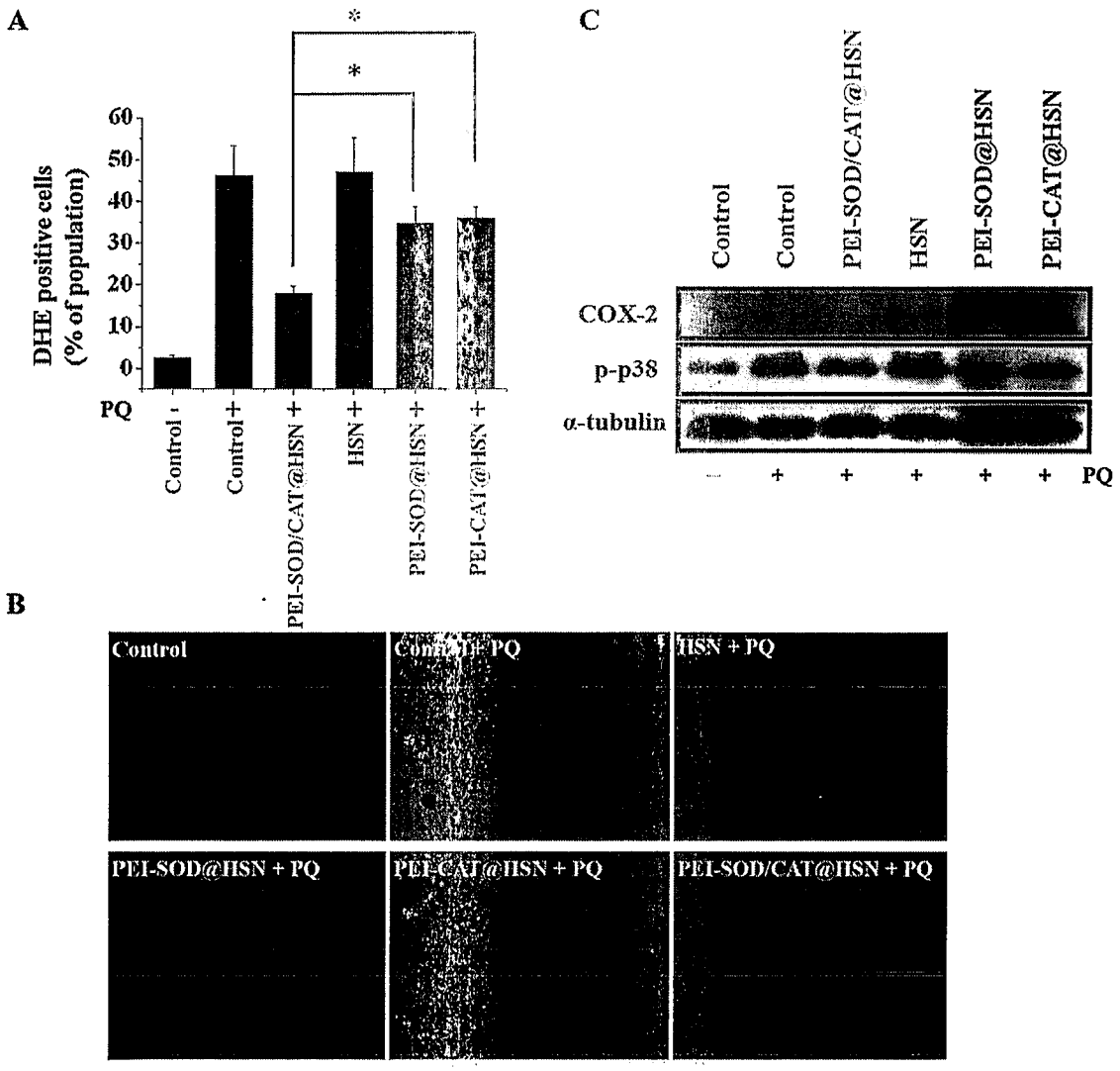

Figure 5. DHE assay and western blotting to evaluate the protective effect of enzyme-loaded particles in cells after PQ treatment. HeLa cells were treated with various particles at a dose of 100 μg mL^{-1}. After 2.5 h, particle-treated cells were further treated with 500 μM of PQ for 18 h. A0 ROS generation determined with DHE by flow cytometry; B) Fluorescence expressions of oxidized DHE by a fluorescence microscope; C) COX-2, p-p38, and α-tubulin expressions by Westernblotting, α-tubulin was used as loading control.

SOD and catalase are co-encapsulated, cascade transformation of superoxide through hydrogen peroxide to water was facile.

Upon cell-uptake of the enzyme-capsulated HSNs, these were shown to function as artificial intracellular organelles for detoxification of superoxides. After delivery to the cells, substantial fractions of HSNs exhibited endosome escape to the cytosol. The cell viabilities were maintained after treatment with HSNs or PEI-SOD/CAT@HSN; indicating no toxicity effect due to the nanoparticles. Upon administering the toxicant paraquat to the cells, both PEI-SOD@HSN and PEI-CAT@HSN showed protective effects to the cells as shown by the decreased ROS production and DHE positive cell counts. The highest cell protection was observed for the co-encapsulated SOD-CAT system. Downstream COX-2 and p-p38 expressions were decreased with treatments of PEI-enzyme@HSN. We have thus shown an effective enzyme-silica nanoreactor system that can be easily uptaken by cells to function as a strong anti-oxidative artificial organelle. Carefully controlling the synthesis[42] and carrying out proper surface functionalization for targeting[43] will result in PEI-SOD/CAT@HSN particles that can be applied as rapid-action antioxidants for many medical treatments, such as for inflammation, ischemia, stroke and other strong oxidative stress situations. We also anticipate further development of HSNs encapsulating other cascade enzyme systems for augmenting cell functions or enzyme therapy using similar approaches.

4. Experimental Section

Modification of SOD and CAT with PEI: PEI-conjugation of enzymes was carried using an NHS/EDC crosslinking reaction. Briefly, 3 mg of SOD and CAT were dissolved in 50 mM sodium phosphate buffer (pH 7.8) at a concentration of 3 mg mL^{-1}. Amine-reactive NHS esters and EDC·HCl were prepared in 200 μL sodium phosphate buffer (50 mM, pH 7.8) and then added to the enzyme solution. The SOD solution contained 17 mg NHS/14 mg EDC·HCl

© 2014 Wiley-VCH Verlag GmbH & Co. KGaA, Weinheim

NANO MICRO small

and the CAT solution contained 15 mg NHS/13 mg EDC·HCl. After stirring for 1 h at 4 °C, 43 and 38 μL of PEI reagent were added to the SOD and CAT solutions, respectively, and the mixtures were further stirred at 4 °C for 24 h to complete the reactions. Finally, the PEI-conjugated SOD (PEI-SOD) and CAT (PEI-CAT) were purified and concentrated with Amicon Ultra filters (MA, USA).

Synthesis of PEI-SOD@HSN, PEI-CAT@HSN, and PEI-SOD/CAT@HSN: Hollow silica nanospheres (HSNs) were synthesized by a reverse microemulsion method.[14,44] Typically, 20 mL of decane, 1.63 mL of CA-520, 550 μL of n-hexanol, and 350 μL of H_2O with concentrated PEI-enzymes (PEI-SOD, PEI-CAT, or a mixture of PEI-SOD and PEI-CAT) were mixed at room temperature to generate the water-in-oil microemulsion. Then, silica sources (100 μL of TEOS and 25 μL of ethanolic APTMS solution) were added with stirring. The ethanolic APTMS solution was prepared by adding 200 mL of APTMS to 1.4 mL of absolute ethanol. After 10 min, 250 μL of aqueous ammonia (35 wt%) was introduced to the mixture, which was then stirred for 10 h at 20 °C. Then, 95% ethanol was added to destabilize the microemulsion system and the solid products were centrifuged at 11 000 rpm for 30 min. To obtain the hollow structure, the samples were suspended in 40 mL warm water (40 °C), stirred for 40 minutes, and isolated by centrifugation to obtain PEI-SOD@HSN, PEI-CAT@HSN, PEI-SOD/CAT@HSN, or HSNs only (without adding enzymes). Finally, all nanoparticles were washed several times with ethanol and deionized water to extract the surfactants in the pores. Previously,[44] we have shown by thermogravimetric analysis (TGA) that most of the surfactants can be removed using this extraction procedure. The amount of PEI-enzymes used to prepare enzyme-loaded HSNs: 36 nmol of PEI-SOD for PEI-SOD@HSN; 4 nmol of PEI-CAT for PEI-CAT@HSN; 36 nmol of PEI-SOD, and 4 nmol of PEI-CAT for PEI-SOD/CAT@HSN.

Synthesis of F-HSN and PEI-SOD/CAT@F-HSN: The green-emitting fluorescein dye (FITC) incorporated in HSNs and PEI-SOD/CAT@HSN (named F-HSN and PEI-SOD/CAT@F-HSN) were synthesized by the aforementioned procedure, except that 25 μL ethanolic FITC-APTMS solution was used instead of 25 μL APTMS ethanolic solution. Ethanolic FITC-APTMS solution was prepared by adding 10 mg of fluorescein isothiocyanate and 200 μL of APTMS to 1.4 mL of absolute ethanol in the dark for 24 h under stirring.

Enzymatic Activity Assays: In the case of SOD, samples were prepared in 300 μL and monitored using a microplate reader (Bio Tek, Synergy H1). First, a stock of cocktail reagent containing ethylenediaminetetraacetic acid (EDTA) (10^{-4} M), cytochrome c (10^{-5} M), and xanthine (5×10^{-5} M) in 1 mL of 50 mM K_3PO_4 was prepared.[45] Then, 280 μL of cocktail reagent was added with various samples (native SOD, PEI-SOD/CAT@HSN, PEI-SOD@HSN, PEI-CAT@HSN, or HSNs), Then, xanthine oxidase (10 μL of 58 mU mL^{-1}) was added to the above solution completed with deionized water up to 300 μL total volume. Finally, 200 μL of each sample was transferred to a microplate reader and the absorbance at 550 nm was determined. To measure the SOD activity, the inhibition rate of cytochrome c reduction between native SOD (3000 U mg^{-1}) and SOD-loaded particles (PEI-SOD/CAT@HSN and PEI-SOD@HSN) were compared using the slopes of absorbance between $t = 0$ s and $t = 180$ s.

In the case of CAT assay, 90 μL of H_2O_2 solution (5 μM in 50 mM sodium phosphate buffer; pH 7.8) and various nanoparticles solutions (native CAT, PEI-SOD/CAT@HSN, PEI-CAT@HSN, PEI-SOD@HSN, or HSNs) were mixed and completed with deionized water up to 100 μL total volume. After incubation for 30 min, HRP (100 μL of 2 U mL^{-1}) and Amplex red (10 μL of 0.1 mM) were added. Each sample (200 μL) was transferred to a microplate reader and the absorbance was monitored at 570 nm. To determine the CAT activity, we calculated the ΔOD_{570} of each sample between $t = 0$ min and $t = 30$ min and compared this with native CAT.

Stability of Encapsulated CAT in the Presence of Superoxide Anions: Native CAT and CAT-loaded HSNs (PEI-SOD/CAT@HSN and PEI-CAT@HSN) were suspended in 50 μL of KO_2 solution (4×10^{-3} mg mL^{-1} in phosphate-buffered saline (PBS)). After incubation for 20 min, each sample was centrifuged with Amicon Ultra filters to remove the KO_2 solution and then re-suspended in 80 μL of H_2O_2 solution (3.75 μM in 50 mM sodium phosphate buffer; pH 7.8). After 30 min, HRP (100 μL of 2 U mL^{-1}) and Amplex red (10 μL of 0.1 mM) were added. Each sample (200 μL) was transferred to a microplate reader and monitored at 570 nm for absorbance. The relative activity of each sample was calculated from the following fitting:

$$\text{Relative activity of each sample} = \frac{\text{The change in absorption at 570 nm } (\Delta OD_{570}) \text{ after } KO_2 \text{ treatment}}{\text{The change in absorption at 570 nm } (\Delta OD_{570}) \text{ before } KO_2 \text{ treatment}} \quad (1)$$

Cascade Reaction of PEI-SOD/CAT@HSN: Enzyme-loaded HSNs, including PEI-SOD@HSN and PEI-SOD/CAT@HSN, and non-enzyme blanks (HSNs only) were suspended in 90 μL of sodium phosphate buffer (50 mM, pH 7.8). Then 10 μL of superoxide solution generated by KO_2 (2 mg mL^{-1} PBS) was added to each sample. After incubation for 30 min at 37 °C, the samples were centrifuged (14 000 rpm, 20 min) and the supernatant was transferred to another Eppendorf. Subsequently, 100 μL of HRP solution (2 U mL^{-1} in H_2O) and 10 μL of Amplex-red reagent (0.1 mM in DMSO) were added and the mixture was further incubated for 5 min. Finally, 200 μL of each sample was transferred to a microplate reader and the amount of H_2O_2 was determined by fluorescence (excitation: 530 nm).

Cell Culture: HeLa cells obtained from the American Type Culture Collection (Manassas, VA) were maintained in Dulbecco's modified Eagle's medium (DMEM; GIBCO) with 10% fetal bovine serum (FBS; GIBCO), 100 U mL^{-1} penicillin, and 100 μg mL^{-1} streptomycin (GIBCO) at 37 °C in a humidified 5% CO_2 atmosphere. When adherent cells reached about 60–70% confluence, they were detached with 0.25% trypsin-EDTA growth medium to allow for continued passaging.

Endosome Escape Examination: Cells were seeded at a density of 2×10^5 cells per well in 6-well plates with cover glasses at the bottom of the wells, and allowed to attach for 24 h. Cells were co-cultured with an endosome marker FM 4–64 (5 μg mL^{-1}) and BSA-stabilized PEI-SOD/CAT@F-HSN and F-HSN (100 μg mL^{-1}) in serum-free medium. After 2.5 h of incubation, the cells were washed twice with PBS and then fixed in a 4% formaldehyde PBS solution at room temperature for 10 min. Then, the treated cells were stained with 4′,6-diamidino-2-phenylindole (DAPI) in PBS (1 μg mL^{-1}) for 10 min at room temperature, washed twice with PBS, and then fluorescence images were obtained with a confocal microscope (TCS SP5, Leica).

Western Blotting Analysis: After each treatment, cell lysates were separated on a 10% SDS-PAGE, and the proteins were then electrophoretically transferred to a polyvinylidene difluoride (PVDF) membrane and blocked 1 h at room temperature

© 2014 Wiley-VCH Verlag GmbH & Co. KGaA, Weinheim

in blocking buffer [1× Tris-buffered saline (TBS)-0.1% Tween 20, 5% w/v non-fat dry milk]. Membranes were incubated overnight at 4 °C with primary antibodies. COX-2 was diluted in TBS-T with 5% w/v milk (1: 500 dilutions; Cayman), p-p38 was diluted in TBS-T with 5% w/v BSA (1: 500 dilutions; Cell Signaling Technology), and α-tubulin was diluted in TBS-T with 5% w/v milk (1:12 000 dilutions; Oncogene Science). PVDF membranes were extensively washed and incubated with a horseradish peroxide-conjugated secondary antibody (1: 2000 dilutions) for 1 h at room temperature. Immuno-reactive bands were visualized with an enhanced chemiluminescence substrate kit (Amersham Pharmacia Biotech, GE Healthcare UK Ltd, Bucks, UK) according to the manufacturer's protocol.

Superoxide Detection: The superoxide anion was fluorometrically estimated using a fluorescent probe, dihydroethidine (DHE), which is oxidized to a fluorescent intercalator, ethidium, by cellular oxidants, in particular, superoxide radicals. Therefore, to measure the superoxide anion generation in our system dihydroethidine (DHE; 5 μM) was used. The increase in DHE fluorescence upon paraquat (superoxide anion generator) stimulation indicated an increase in superoxide anion levels. After various experimental treatments, fluorescence images were obtained with a fluorescence microscope (IX-71, Olympus) and quantitative data were analyzed with a FACS Calibur flow cytometer.

Supporting Information

Supporting Information is available from the Wiley Online Library or from the author.

Acknowledgements

This research was funded by the National Taiwan University and the Ministry of Science and Technology (MOST) of Taiwan. We thank Chia-Ying Chien for assistance with the TEM experiments, Dr. Fan-Ching Chien (National Central University, Taiwan) for assistance with the confocal microscopy, and Jen-Hsuan Chang for help in the initial study.

[1] C. G. Palivan, O. Fischer-Onaca, M. Delcea, F. Itel, W. Meier, *Chem. Soc. Rev.* **2012**, *41*, 2800.
[2] P. Tanner, S. Egli, V. Balasubramanian, O. Onaca, C. G. Palivan, W. Meier, *FEBS Lett.* **2011**, *585*, 1699.
[3] P. Walde, S. Ichikawa, *Biomol. Eng.* **2001**, *18*, 143.
[4] R. J. R. W. Peters, M. Marguet, S. Marais, M. W. Fraaije, J. C. M. van Hest, S. Lecommandoux, *Angew. Chem., Int. Ed.* **2014**, *53*, 146.
[5] H. Baumler, R. Georgieva, *Biomacromolecules* **2010**, *11*, 1480.
[6] S. F. M. van Dongen, M. Nallani, J. L. L. M. Cornelissen, R. J. M. Nolte, J. C. M. van Hest, *Chem.-Eur. J.* **2009**, *15*, 1107.
[7] P. Tanner, O. Onaca, V. Balasubramanian, W. Meier, C. G. Palivan, *Chem.-Eur. J.* **2011**, *17*, 4552.
[8] S. A. Meeuwissen, A. Rioz-Martinez, G. de Gonzalo, M. W. Fraaije, V. Gotor, J. C. M. van Hest, *J. Mater. Chem.* **2011**, *21*, 18 923.
[9] D. M. Vriezema, P. M. L. Garcia, N. S. Oltra, N. S. Hatzakis, S. M. Kuiper, R. J. M. Nolte, A. E. Rowan, J. C. M. van Hest, *Angew. Chem., Int. Ed.* **2007**, *46*, 7378.
[10] W. Siti, H. P. M. de Hoog, O. Fischer, W. Y. Shan, N. Tomczak, M. Nallani, B. Liedberg, *J. Mater. Chem. B* **2014**, *2*, 2733.
[11] M. Marguet, C. Bonduelle, S. Lecommandoux, *Chem. Soc. Rev.* **2013**, *42*, 512.
[12] X. L. Wang, Z. Li, J. F. Shi, H. Wu, Z. Y. Jiang, W. Y. Zhang, X. K. Song, Q. H. Ai, *ACS Catal.* **2014**, *4*, 962.
[13] F. P. Chang, Y. Hung, J. H. Chang, C. H. Lin, C. Y. Mou, *ACS Appl. Mater. Interfaces* **2014**, *6*, 6883.
[14] S. H. Wu, C. T. Tseng, Y. S. Lin, C. H. Lin, Y. Hung, C. Y. Mou, *J. Mater. Chem.* **2011**, *21*, 789.
[15] F. Chen, H. Hong, Y. Zhang, H. F. Valdovinos, S. Shi, G. S. Kwon, C. P. Theuer, T. E. Barnhart, W. Cai, *ACS Nano* **2013**, *7*, 9027.
[16] J. M. Rosenholm, V. Mamaeva, C. Sahlgren, M. Linden, *Nanomedicine* **2012**, *7*, 111.
[17] S. P. Hudson, R. F. Padera, R. Langer, D. S. Kohane, *Biomaterials* **2008**, *29*, 4045.
[18] M. Perez-Lorenzo, B. Vaz, V. Salgueirino, M. A. Correa-Duarte, *Chem. Eur. J.* **2013**, *19*, 12 196.
[19] C. J. Tsou, C. Y. Chu, Y. Hung, C. Y. Mou, *J. Mater. Chem. B* **2013**, *1*, 5557.
[20] C.-J. Tsou, Y. Hung, C.-Y. Mou, *Microporous Mesoporous Mater.* **2014**, *190*, 181.
[21] W. I. Lin, C. Y. Lin, Y. S. Lin, S. H. Wu, Y. R. Huang, Y. Hung, C. Chang, C. Y. Mou, *J. Mater. Chem. B* **2013**, *1*, 639.
[22] Y. Chen, H. R. Chen, J. L. Shi, *Acc. Chem. Res.* **2014**, *47*, 125.
[23] Y. Chen, H. Chen, L. Guo, Q. He, F. Chen, J. Zhou, J. Feng, J. Shi, *ACS Nano* **2010**, *4*, 529.
[24] Y. Chen, H. R. Chen, J. L. Shi, *Adv. Mater.* **2013**, *25*, 3144.
[25] Y. Chen, H. Chen, D. Zeng, Y. Tian, F. Chen, J. Feng, J. Shi, *ACS Nano* **2010**, *4*, 6001.
[26] P. Nicholls, I. Fita, P. C. Loewen, *Adv. Inorg. Chem.* **2001**, *51*, 51.
[27] E. Hood, E. Simone, P. Wattamwar, T. Dziubla, V. Muzykantov, *Nanomedicine* **2011**, *6*, 1257.
[28] P. Tanner, V. Balasubramanian, C. G. Palivan, *Nano Lett.* **2013**, *13*, 2875.
[29] Y. Chen, P. Xu, H. Chen, Y. Li, W. Bu, Z. Shu, J. Zhang, L. Zhang, L. Pan, X. Cui, Z. Hua, J. Wang, J. Shi, *Adv. Mater.* **2013**, *25*, 3100.
[30] J. Futami, M. Kitazoe, T. Maeda, E. Nukui, M. Sakaguchi, J. Kosaka, M. Miyazaki, M. Kosaka, H. Tada, M. Seno, Y. Sasaki, N. H. Huh, M. Namba, H. Yamada, *J. Biosci. Bioeng.* **2005**, *99*, 95.
[31] W. T. Godbey, K. K. Wu, A. G. Mikos, *J. Controlled Release* **1999**, *60*, 149.
[32] A. C. Hunter, *Adv. Drug Delivery Rev.* **2006**, *58*, 1523.
[33] S. M. Moghimi, P. Symonds, J. C. Murray, A. C. Hunter, G. Debska, A. Szewczyk, *Mol. Ther.* **2005**, *11*, 990.
[34] H. Meng, M. Liong, T. Xia, Z. Li, Z. Ji, J. I. Zink, A. E. Nel, *ACS Nano* **2010**, *4*, 4539.
[35] R. C. Bray, S. A. Cockle, E. M. Fielden, P. B. Roberts, G. Rotilio, L. Calabres, *Biochem. J.* **1974**, *139*, 43.
[36] N. Hadzi-Petrushev, N. Jankulovski, M. Milev, P. Filipovska, H. Gagov, E. Gjorgievska, D. Mitrov, R. Sopi, K. Hristov, M. Mladenov, *J. Therm. Biol.* **2012**, *37*, 361.
[37] B. R. Lokesh, M. L. Cunningham, *Toxicol. Lett.* **1986**, *34*, 75.
[38] Y. Kono, I. Fridovich, *J. Biol. Chem.* **1982**, *257*, 5751.
[39] D. R. Bickers, M. Athar, *J. Invest. Dermatol.* **2006**, *126*, 2565.

 © 2014 Wiley-VCH Verlag GmbH & Co. KGaA, Weinheim

NANO MICRO small

[40] Y. C. Fang, Y. P. Chen, C. T. Chen, T. S. Lin, C. Y. Mou, *J. Mater. Chem. B* **2013**, *1*, 6042.
[41] Q. Yu, T. Wang, X. Zhou, J. Wu, X. Chen, Y. Liu, D. Wu, Q. Zhai, *PLoS One* **2011**, *6*, e21770.
[42] S.-H. Wu, C.-Y. Mou, H.-P. Lin, *Chem. Soc. Rev.* **2013**, *42*, 3862.
[43] S. H. Cheng, C. H. Lee, M. C. Chen, J. S. Souris, F. G. Tseng, C. S. Yang, C. Y. Mou, C. T. Chen, L. W. Lo, *J. Mater. Chem.* **2010**, *20*, 6149.
[44] Y.-S. Lin, S.-H. Wu, C.-T. Tseng, Y. Hung, C. Chang, C.-Y. Mou, *Chem. Commun.* **2009**, 3542.
[45] J. M. McCord, I. Fridovich, *J. Biol. Chem.* **1969**, *244*, 6049.

Received: May 30, 2014
Revised: July 14, 2014
Published online: August 26, 2014

© 2014 Wiley-VCH Verlag GmbH & Co. KGaA, Weinheim

A general approach to co-deliver two denatured antioxidant enzymes by using MSN for a series nanoreaction in cells.

Introduction

In biological system, the addition effect is available mediated at through the interaction between the two proteins with short distance. Two closed enzymes are play a catalytic reaction in a space limitation that is called "cascade reaction". No matter addition or cascade reaction, the distance is a critical point for an efficiency enzymatic reaction in cells. Recently, we reported a microemulsion-template method for synthesizing hollow silica nanospheres (HSNs) for loading two antioxidant enzymes, SOD and Catalase, in the cavity to carry out intracellular cascade transformation of superoxide anion through hydrogen peroxide to water was facile(small 2014, 10, No. 22, 4785–4795). But, the size of many biological enzymes are significantly bigger than the inner space of HSNs or the loading efficiency is limitative. Using individual nanoparticles to delivery two or multi denatured enzymes whether could overcome all the limitations, including size, space, loading efficiency, chemical solvents, and protein unstable, is still unclear (Analyst, 2012, 137, 4435–4439; Biomacromolecules, Vol. 7, No. 1, 2006; Chem. Eur. J. 2009, 15, 1170-1114; Angew. Chem. Int. Ed. 2014, 53, 146 –150).

In fact, as reported previously (J. Am. Chem. Soc. 2013, 135, 1516–1523), we have developed a denatured protein delivery system which combined a MSN nanoparticle carrier and TAT-SOD fusion protein. The combination between nanomaterial and genetic engineer not only overcomes the limitation of protein delivery, including chemical solvents, stability, and permeability, but provide a newly method for protein therapy. In addition, our benefit is the TAT-SOD fusion protein, after *E.coli* overexpression, was conjugated, purified and isolated by using FMSN-NTA-Ni via a one-step metal affinity binding at the same time in the 10 % glycerol buffer. After the protein denaturation of TAT-SOD conjugated FMSN (FMSN-TAT-SOD) in 8M urea, the TAT-SOD fusion protein was refolded and exhibited specific activity in cells.

Although a very usefully method with a smartly procedure has been established, it is not sufficient for its potential and application. Thus, it is necessary to develop the following requirements: (i) it should be more simple, that is, one-step isolation, conjugation and protein denaturation could be achieved in 8M urea at the same times; (ii) it should be also suitable for another protein especially for the different

expressing type's protein; and (iii) it should be capable of two or multi enzymes delivery to regulate cellular function by a nanoreacting in cells. To address the challenge and promote the promising system, in this study we further improved on extending the applicability for different expressing types of protein delivery and co-delivery of two denatured proteins by nanoparticles as a nanoreactor in cells. Hence, we chose two antioxidant proteins with similar function for free radicals scavenging, superoxide dismutase (SOD) and glutathione peroxidase (GPx), to be demonstrated.

In prokaryotic protein expression system, genetic protein by molecular cloning often was expressed in the supernatants (supernatant's type) or pellets (pellet's type) of *E. coli* crude lysates based on their property. For example, SOD is a metalloprotein expressed in the supernatants (mainly) and pellet (partly) (Ann. N.Y. Acad. Sci. 2005 1042 303–313). GPx, a special selenium-protein, was only mainly expressed and precipitated in the *E. coli* pellets. The pellet's type overexpression protein is a trouble in preparation; N-Lauroylsarcosine (sarkosyl) was common used to lysis the *E. coli* pellets and stable the expression protein activity, according to standard purification procedure of prokaryotic overexpressed protein system (Meth Enzymol. 1996 273 144–145.). Therefore, the propose was to establish a procedure to verify that two kinds of genetic engineering protein containing supernatant or pellet's types could be apply in this improved system to become more easily and quickly preparation, without having to separate what types of protein were overexpressed in *E.coli*. On the basis of the results shown in this paper, it has been examined that the pellets of *E. coli* crude lysates expressed TAT-SOD or TAT-GPx could be directly lysed and conjugated by adding FMSN-NTA-Ni nanoparticles under 8M urea condition. Finally, the TAT-SOD or TAT-GPx protein functionalized FMSN, named as FMSN-TAT-SOD or FMSN-TAT-GPx, was denatured and isolated at the same time after centrifugation. In addition, our results displayed that FMSN-TAT-SOD or FMSN-TAT-GPx through this procedure preparation also have enzymatic activity by refolding mechanism in cells as well as our previous report's method for FMSN-TAT-SOD. Along with these finding, this improved system not only reserved original benefit such as sensitive by metal affinity binding, but provided a more quickly, simpler and easy method to achieve the denaturation, conjugation and purification at the same time by 8M urea. Here, the purified TAT-SOD or TAT-GPx proteins on FMSN could be dissociated by adding excessive imidazole for further identification and protein assay. The most important is that we show the system is general and able to apply in different types of overexpressed protein by genetic engineering.

Cellular uptake of nanoparticles is divided into energy-independent (non-endocytosis) and energy-dependent (endocytosis) routes. Endocytosis is a major cell uptake mechanism which involved in different pathway such as caveolae-mediated, clathrin-mediated and micropinocytosis (NAT REV DRUG DISCOV 2010, 9, 615-627; Nature 2003, 422, 37-44). In general, most of nanoparticles internalized with cell membrane to form vesicles by endocytosis pathway, following the vesicles were trapped in endosome/lysosome and moved along the cytoskeleton such as microtubule (MT) into the microtubule-organizing center (MTOC) by kinesin and dynesin (J. AM. CHEM. SOC. 2007, 129, 14759-14766; Chem. Soc. Rev., 2011, 40, 233-245; J Cell Biol. 2000, 150(5), 111–116; Nano Lett., 2014, 14 (5), pp 2515–2521). In particular, Wang and co-workers found the interaction between TAT peptide and cytoskeleton (PNAS 2011 108 (41) 16883-16888; PNAS 2007, 104,20805-), indicating TAT peptide not only internalized by endocytosis, but interact with the membrane to generate pore-like structure. Importantly, TAT has strong interaction with actin which can remodel the cytoskeleton. Besides, TAT peptide also provide a non-endocytosis delivery, endosome escape and proton sponge effect that could enhance the efficiently nanoparticles delivery (Pharmaceuticals. 2012, 5(11), 1177–1209.).

However, to the best of our knowledge, by using individual nanoparticles to delivery two or multi denatured enzymes as a nanoreaction in cells has not been reported in literature. In this study, we fabricated MSN conjugated with two different types of proteins and then co-delivered into cells to investigate effects of individual nanoparticles on the addition reaction in cells. We hypothesized that there nanoparticles, when they were moving and aggregating along the cytoskeleton into the MTOC after the delivery, were not only trapped in endosome, but escaped by TAT peptides that would allow them to very close to each other at same time, result in increasing the cellular addition reaction. Therefore, the two proteins have more probability to promote the nanoreaction duo to the short distance by nanoparticles strategy.

2. Results and Discussion

For TAT-SOD and TAT-GPX Proteins conjugation, we constructed and overexpressed the His-tag human Cu, Zn-superoxide dismutase (SOD) and human glutathione peroxidase (GPx) which contain a human immunodeficiency virus (HIV) transducing domain (TAT, 49-57)(Ann. N.Y. Acad. Sci. 2005 1042 303–313). The genes of TAT-SOD and TAT-GPx were cloned and inserted into prokaryotic protein expression vector of pQE-30 to form pQE-TAT-SOD and pQE-TAT-GPx (Fig 1a). The vectors were transformed into JM109 *E. coli* and cultured in LB broth with IPTG protein induction for 1 and 3 h. The TAT-SOD and TAT-GPx with high protein overexpression were displayed in accordance with increasing induction time in 10 % SDS-PAGE electrophoresis (Fig S1). To identify the overexpressed protein distribution, we separated *E.coli* crude lysates in the supernatants (supernatant's type) and pellets (pellet's type) by centrifugation after the IPTG induction for 3h. Then, the pellets of *E. coli* crude lysates were treated with 8M urea to dissolve the pellets and following to collect its supernatants after centrifugation. 10 % SDS-PAGE analysis revealed TAT-SOD was overexpressed in the *E. coil* supernatants (mainly) and pellets (partly). However, TAT-GPx significantly belonged to the pellets types of overexpressed protein (Fig 1b). Finally, the supernatants of pellets of *E. coli* crude lysates expressed TAT-SOD or TAT-GPx were tried to further directly conjugate in 8M urea.

FITC conjugated MSN (FMSN) was synthesized according to our previously reported methods (J. Am. Chem. Soc. 2013, 135, 1516−1523). The NTA-Ni tethers were conjugated onto FMSN to form FMSN-NTA-Ni with an average loading of Ni content is 0.6 wt % by ICP-MS analysis. Based on the metal affinity between the Ni (II) and His-tag protein offered a tight linkage with a very low dissociation constant, the FMSN-NTA-Ni was directly mixed with TAT-SOD or TAT-GPx proteins from the supernatants of pellets of *E. coli* crude lysates under 8M urea without purifying. TEM images show that these MSN particles possess well-ordered mesoporous structure with an average particle size are ~ 50 nm (Figure 1c). DLS-determined size indicates slight aggregation in solution (Table S1). In addition, the concentration of TAT-SOD or TAT-GPx functionalized on FMSN-NTA-Ni was determined by Bradford assay by measuring the supernatants through the 500 mM of imidazole digested the linkage between the NTA-Ni and His-tag. We found the weight percent of TAT-SOD and TAT-GPx on FMSN was 1.19 wt% and 1.22 wt%, respectively. The dissociated TAT-SOD or TAT-GPx proteins from nanoparticles were identify by using Western blotting (Fig 1d). In brief, this method is able to not only contain the original benefit of one-step conjugation and easy purification, but become simpler conjugation because the pellets of E. coli crude lysates expressed TAT-SOD or TAT-GPx were directly lysed in 8M urea after the protein overexpression.

In this study, our strategy is to deliver the TAT-fusion denatured enzymes into cells. To verify the FMSM-TAT-SOD or FMSN-TAT-GPx which is able to delivery into HeLa cells, 25-250 μg/mL of FMSM-TAT-SOD or FMSN-TAT-GPx was added to the DMEM and incubated with HeLa cells for 4 h. Then, harvested cells were lysed with RIPA buffer containing 500 mM imidazole for protein digestion from FMSN surface. Western blotting of cell lysates was separately used to carry out the levels of cellular SOD and GPx, which indicated both FMSN-TAT-SOD and FMSN-TAT-GPx have been efficiently transduced into the HeLa cells in a dose-dependent manner (Fig 2a). Flow cytometry analysis was further utilized to quantitatively evaluate the cellular uptake of FMSM-TAT-SOD or FMSN-TAT-GPx. After the treatment of HeLa cells with different concentrations of nanoparticles (25-250 μg/mL) for 4 h, the surface FITC fluorescence signal of trypsinized cells was quenched by adding trypan blue for flow cytometric assay. Not surprisingly, the cell uptake percentages were increased in accordance with concentrations in HeLa cells following treatment with FMSN-TAT-SOD and FMSN-TAT-GPx. Obviously, the saturation concentrations of FMSN-TAT-SOD and FMSN-TAT-GPx were 100 μg/mL and 50 μg/mL that reached about 80 % and 60 % uptake percentage, respectively. (Fig 2b). At the same condition, the cytotoxicity of FMSN-TAT-SOD or FMSN-TAT-GPx on HeLa cells was examined. By using WST-1 assay, figure S2 shown that FMSN-TAT-SOD or FMSN-TAT-GPx didn't significantly reduce the cell viability, indicating protein functionalized FMSN have good cell biocompatibility.

According to our previous report (J. Am. Chem. Soc. 2013, 135, 1516−1523), we have demonstrated that denatured TAT-SOD on FMSN could be refolded successfully in HeLa cells with good cellular SOD specific activity in a dose-dependent manner. In this study, we hypothesized that HeLa cells, when co-delivery of TAT-SOD and TAT-GPx, might exert a stronger addition effect. Hence, the restoration of enzymatic activities of TAT-SOD and TAT-GPx in cells became a crucial point for this purpose. To address this, FMSN-TAT-SOD and FMSN-TAT-GPx were delivered into HeLa cells and the specific activity was carried out, respectively (Fig 2c). As expected, FMSN-TAT-SOD exhibited SOD activity via a dose-dependent manner. However, we found the FMSN-TAT-GPx activity was saturated over the 50 μg/mL of nanoparticles, resulting in the excess GPx might aggregate in cells to form inclusion body with the loss of activity. We also considered the probability that the decreased activity was caused through protein degradation or other intracellular mechanisms.

As described, both of the TAT-SOD and TAT-GPx proteins could delivery into HeLa cells and restore their activity. These enzymes are famous antioxidant enzyme which are involved in scavenge free radicles in cells for protecting cell to against ROS induced stress. To evaluate their potential as ROS scavenger, paraquat (N,

N'-dimethyl-4, 4'-bipyridinium dichloride, PQ), a specific superoxide anion generator, was used to induce superoxide anion ($\cdot OH^-$) production. First, we treated with different concentrations of FMSN-TAT-SOD or FMSN-TAT-GPx for 4 h, then added 500 μM of PQ for another 24 h. The protection ability was determined by the cell viability by WST-1 assay. Figure 2d showed that the treatment with FMSN-TAT-SOD or FMSN-TAT-GPx significantly increased the cell viability compared with control FMSN-NTA-Ni. Although FMSN-TAT-SOD or FMSN-TAT-GPx enhanced cell viability in a dose-dependent manner, FMSN-TAT-GPx still had better ability to protect PQ induced ROS damage than FMSN-TAT-SOD. One of reasons is FMSN-TAT-GPx plays a role in quickly remove the hydrogen peroxide to avoid the Fenton and Haber-Weiss reaction generated the hydroxyl radical ($\cdot OH^-$) (Science, 1998, 240, 640-642). Besides, control FMSN-NTA-Ni exhibited a slight effect duo to the mesoporous structure might adsorb part of superoxide anion or paraquat directly in cells.

As we know, SOD and GPx are powerful up-downstream antioxidant enzymes and defense ROS in the living cells (Eur. J. Biochem. 1993, 215, 213-219). This property acts as a suitable model to study the potential about nanoparticles based nanoreaction by two enzymes co-delivery. For a better understanding, we therefore co-delivered TAT-SOD and TAT-GPx functionalized FMSN into HeLa cells. In order to investigate the addition reaction could be occurred mediated at through the co-delivery of FMSN-TAT-SOD and FMSN-TAT-GPx, we fixed the total particles weight (50 μg/mL) and chose the ratio (1:1) of SOD and GPx (FMSN-TAT-SOD: 25 μg/mL; FMSN-TAT-GPx: 25 ug/mL) to observe whether the combination was available for enhancing cell viability after the PQ treatment. Figure 3a indicated that co-delivery of FMSN-TAT-SOD and FMSN-TAT-GPx had more efficiency for reducing ROS induced cell damage as compared to 25 or 50 ug/mL of single protein delivery. The single protein delivery, either 25 ug/mL of FMSN-TAT-SOD or FMSN-TAT-GPx, only slightly enhance the cell viability. Obviously, the addition reaction which was occurred via co-deliver of FMSN-TAT-SOD and FMSN-TAT-GPx (ratio: 1:1) significantly helped cells to against the stress. However, nether 50 ug/mL of FMSN-TAT-SOD nor FMSN-TAT-GPx delivery also could not effect batter than the co-delivery. To further verify the hypothesis of addition reaction for ROS protection, we tested the assumption by quantitating ROS. ROS was stained with dihydroethidine (DHE) (J. Neurosci., 1996, 16(4), 1324-1336) after the co-delivery with PQ treatment following detection by flow cytometry. As compared with figure 3a, we found the same results that the co-delivery of FMSN-TAT-SOD and FMSN-TAT-GPx had the best ability for scavenging ROS. As described above, we are the first to demonstrate the nanoparticles based co-delivery of two up-downstream enzymes may contribute the metabolic benefit in sequential catalytic reactions.

After treated with the co-delivery of FMSN-TAT-SOD and FMSN-TAT-GPx and PQ, we also imaged the ROS production by using fluorescence microscopy. Results observed in Figure 3c showed less red fluorescence indicated the endogenous ROS in HeLa cells without treatment. In contrast, the red fluorescence dramatically increased after cells were treated with 500μM PQ. While the treatment with co-delivery of FMSN-TAT-SOD and FMSN-TAT-GPx (ratio: 1:1), the red fluorescence dramatically disappeared, indicating a significant declining of ROS level. Subsequently, the effect of co-delivery of FMSN-TAT-SOD and FMSN-TAT-GPx (ratio: 1:1) on the percentages of cell cycle phase (G1, S and G2/M) were quantified by flow cytometry. The results of cell cycle distribution (fig. 3d) displayed PQ induced S phase arrest that indicated cells can't process from mitosis into G2/M phase. In contrast, as the control, FMSN was ineffective. PQ induced S phase arrest could be progressed when the FMSN-TAT-SOD and FMSN-TAT-GPx were co-delivered into cells, suggesting all the phases were recovered. Thus, the promoting proliferation property of the co-delivery of FMSN-TAT-SOD and FMSN-TAT-GPx (figure 3a) could be attributed to increasing cell cycle progression.

Because intracellular ROS could induce cell damage and turn on different signal pathways, we wonder if the p-p38 and COX II proteins expression level could be up-regulated in HeLa cells. Western blot assay resolved the protein expression levels and α-tubulin was used as a loading control. As a stress-activated mitogen-activated protein kinase (MAPK) pathway, p-p38 protein is an important biomarker to detect and respond to intracellular oxidative stress (J Biol Chem., 2004, 279(19), 20451-20460). Additionally, Cyclooxygenase II (COX II), a mainly inflammation biomarker, is induced by ROS (Diabetes, 2003, 52, 2570-2577). From the western blotting results of Figure 3e, the expression level of p-p38 and COX II in HeLa cells could be activated after treating with PQ. But, control FMSN didn't inhibit the higher level expression of COX II and p-p38 under the PQ treatment. Co-delivery of FMSN-TAT-SOD and FMSN-TAT-GPx (ratio: 1:1) exhibited good protection ability to decrease the PQ induced p-p38 and COX II protein expression. Importantly, this result was similar to cell cycle result in figure 3d. In conclusion, our results demonstrated that nanoparticles based protein co-delivery is potential and the addition reaction can be occurred.

Based on our previous report that TAT peptides of FMSN-TAT-SOD expressed by genetic engineering provided an efficiently delivery via the pathway of non-endocytosis or endosome escape mechanism as well as chemical synthesized TAT conjugated nanoparticles (J. Am. Chem. Soc. 2013, 135, 1516−1523). The purpose of the present study was investigated the internalization mechanism of FMSN-TAT-SOD on the pathway of endo- or non-endocytosis (Figure 4a). Endocytosis

is a mainly energy-dependent pathway when cells uptake nanoparticles. We removed energy by low temperature (4℃) (J Biol Chem., 1981, 256(6), 2615-2617) or by the treatment with sodium azide and 2-deoxyglucose (ATP depletion) (J Cell Biol., 1990, 111(6), 2307-2318), suggesting there were only 40 % FMSN-TAT-SOD through non-endocytosis uptake compared to controls. Filipin III has been reported to specifically block caveolae-mediated uptake (MOLECULAR THERAPY Vol. 8, No. 2, August 2003). The uptake of FMSN-TAT-SOD was reduced by 40% under the Filipin III treatment. No significant effect was observed on the uptake of FMSN-TAT-SOD with the treatment of chlorpromazine, an inhibitor of clathrin-mediated pathway (The Journal of Cell Biology, Volume 123, 1993). However, while the treatment with amiloride, a well-known macropinocytosis inhibitor (J. Cell Biol. Vol. 188 No. 4 547–563), the uptake of FMSN-TAT-SOD was reduced by approx. 30%. Taken together, our data revealed that FMSN-TAT-SOD was internalized by cells via an energy-independent and dependent (caveolae-mediated endocytosis and macropinocytosis) process (Nature Medicine, 2004, 10, 310 - 315).

In an effort to explore why the addition phenomenon could be observed in Figure S3. HeLa cells were co-delivered with FITC labeled FMSN-TAT-SOD and FMSN-TAT-GPx (ratio: 1:1) for 4h and stained with SOD (Alexa-568, blue) and GPx (Alexa-647, red). Confocal microscopy imaged both nanoparticles could enter HeLa cells with good uptake (Fig S3 a-c). As shown in Fig S3d, the merge images (cyan) indicated TAT-SOD (blue) was co-localized with FMSN (green). The merge images (yellow) displayed the overlapping of FMSN (green) and TAT-GPx (blue) in Fig S3e. The results of fig S3d-e revealed both proteins were conjugated on the FMSN in HeLa cells. It is worth noting that part of FMSN-TAT-SOD and FMSN-TAT-GPx were co-localized in the cytoplasm from the co-localization images of FMSN (green), TAT-SOD (blue) and TAT-GPx (red) that could explain why the addition reaction might be occurred (as the white arrows indicated in Figure S3f). To more detail confirm the phenomenon, TAT-SOD and TAT-GPx were separately conjugated with different fluorescence nanoparticle (FITC-MSN-SOD and RITC-MSN-GPx) to trace the distribution. Super-resolution (SR) localization microscopy is a class of techniques that enhance the spatial resolution of an imaging system. Thus, after the co-delivery into HeLa cell, direct stochastic optical reconstruction microscopy (dSTORM), one kind of super-resolution localization microscopy was utilized to observe the distribution of FMSN-TAT-SOD (FITC-labeled, green), RMSN-TAT-GPx (RITC-labeled, red) and α-tubulin (Alexa fluor 647-labeled, blue) with a nanoscale imaging resolution of 25 nm (Cell Cycle 11, 3611-3626 (2012).). As shown in Figure 4b, we saw lots of nanoparticles were moving and aggregating along the α-tubulin via an endocytic mechanism; the images revealed yellow dots on the α-tubulin, which indicate co-localization of FMSN-TAT-SOD and RMSN-TAT-GPx.

These nanoparticles could escape from endosome by TAT peptides for promoting the nanoreaction. Besides, part of nanoparticles which were not distributed on the α-tubulin still could observe the colonialization of FMSN-TAT-SOD and RMSN-TAT-GPx through a non-endocytic mechanism. In brief, we demonstrated that the cascade reaction are available by co-delivery of two denatured up-downstream enzymes by nanoparticles.

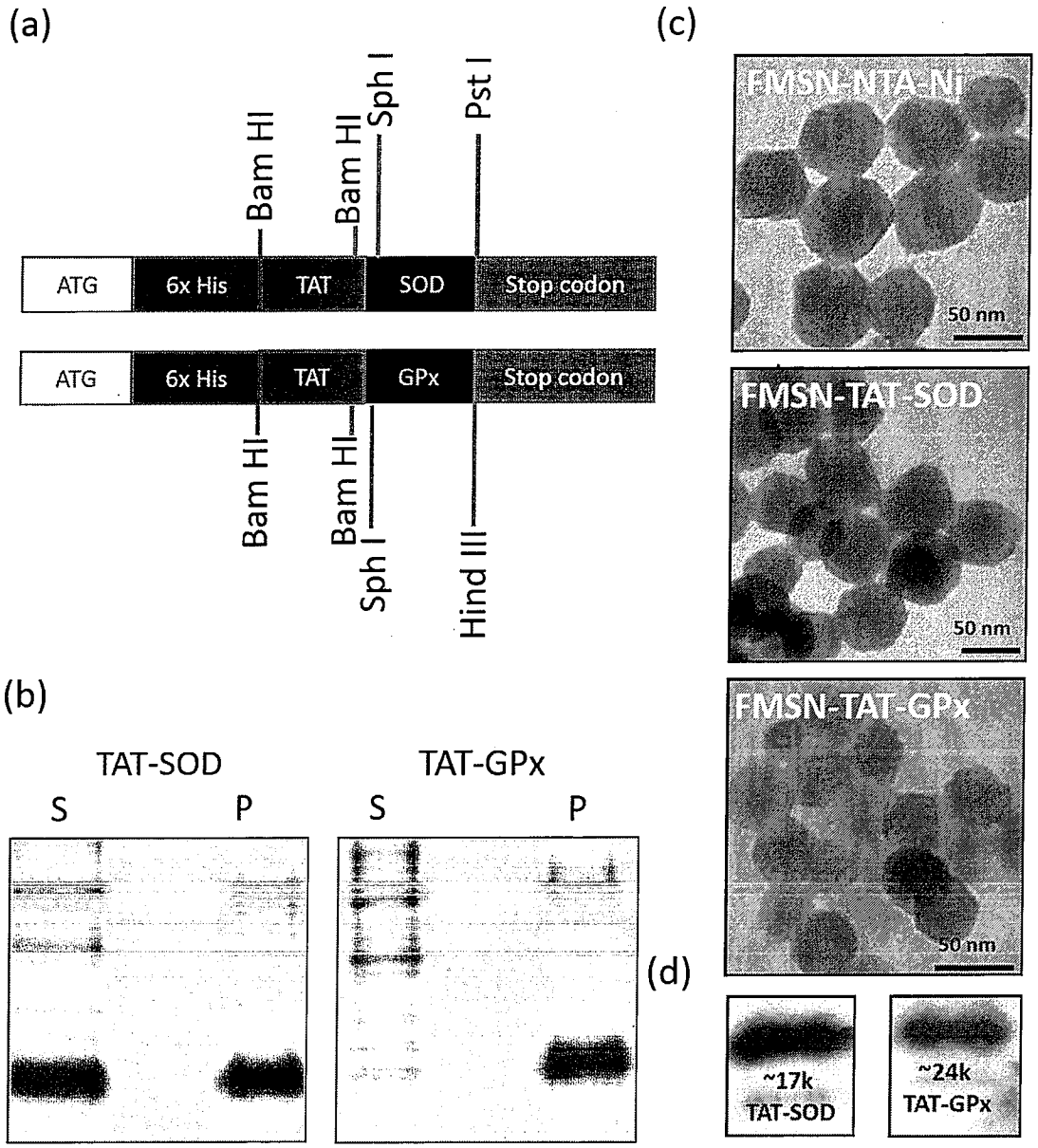

Fig 1. Characterization of Nanoparticles. (a) The gene construct of pQE-TAT-vectors. (b) The isolation of crude lysates from *E.coli* overexpression proteins in 10% SDS-PAGE. S: supernatants; P: pellets. (c) TEM images. (d) Protein identified by using Western blotting. After the protein conjugation, TAT-SOD or TAT-GPx proteins were dissociated from FMSNs via 500 mM of imidazole digestion.

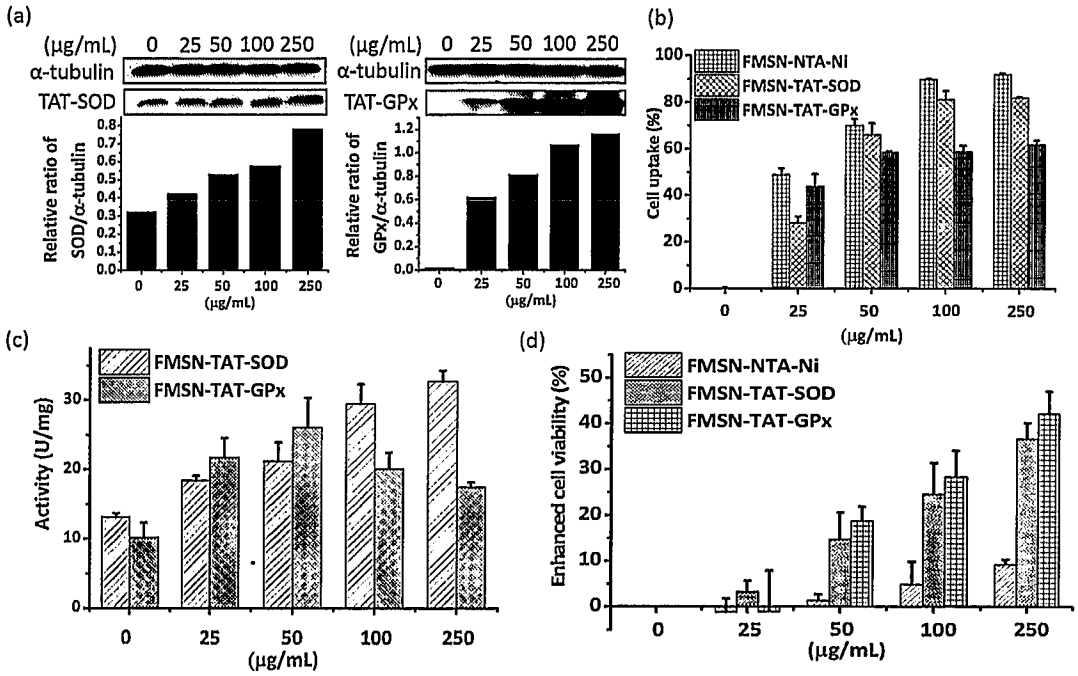

Fig 2. HeLa cells were treated with different concentrations of FMSN-TAT-SOD and FMSN-TAT-GPx (25-250 μg/ml) for 4h. (a) Western blot results for intracellular SOD and GPx levels. (b) Cellular uptake efficiency. (c) Enzymes activity assay. (d) The protection ability of FMSN-TAT-SOD and FMSN-TAT-GPx under 500 μM of paraquat treatment by using WST-1 assay.

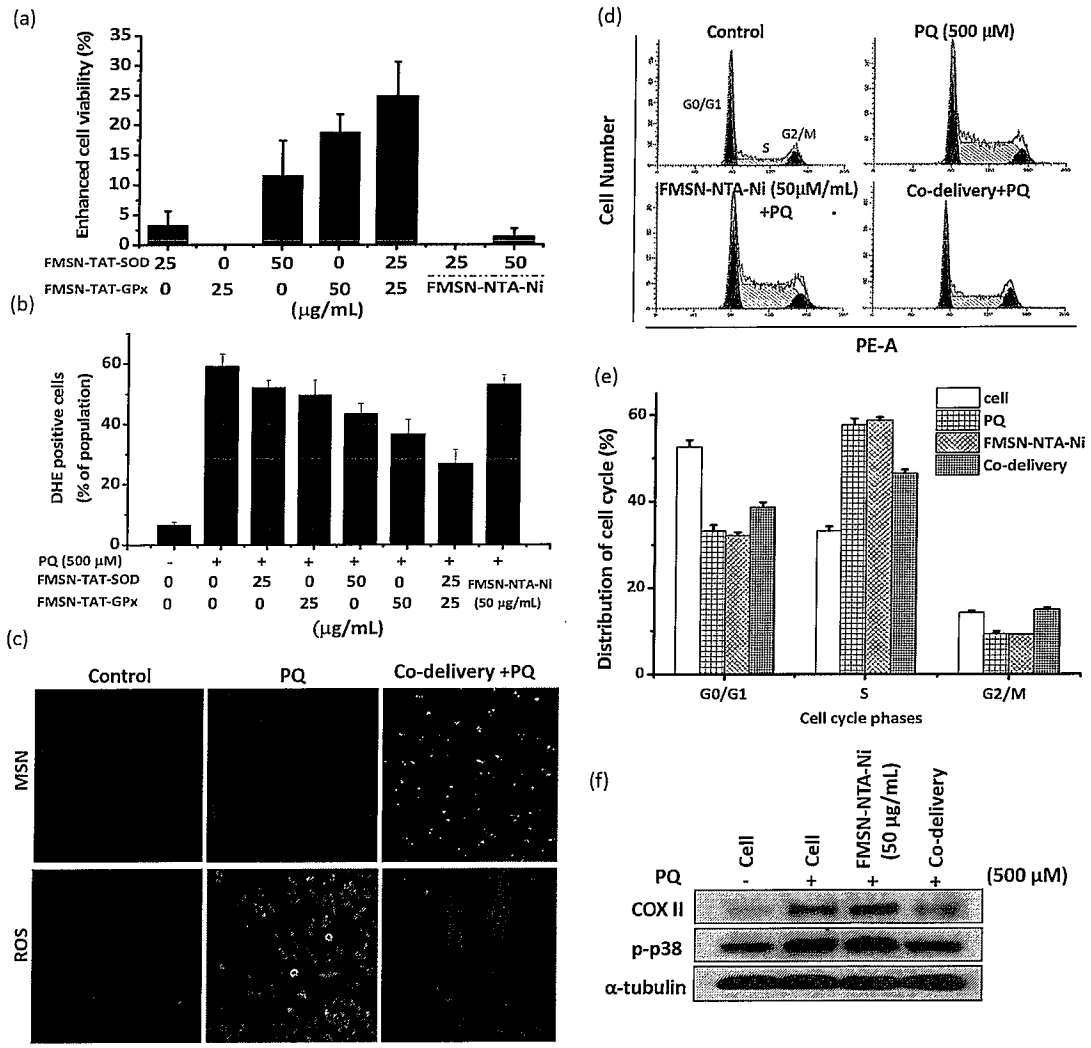

Fig 3. The protection effect of co-delivery of TAT-SOD and TAT-GPx into Hela cells. (a) Enhanced cell viability by using WST-1 assay. (b) ROS detection. The levels of ROS were stained by DHE assays and quantified by flow cytometry. (c) Fluorescence microscopy images the ROS expression. (d) Cell cycle analyses. The graphs of figure 3e are representative of the three independent experiments, each showing similar results. (e) Western blotting assays of the levels of COX II and p-p38. The concentration of PQ and co-delivery of FMSN-TAT-SOD and FMSN-TAT-GPx (1:1 ratio) are 500 μM and 25 μg/mL, respectively.

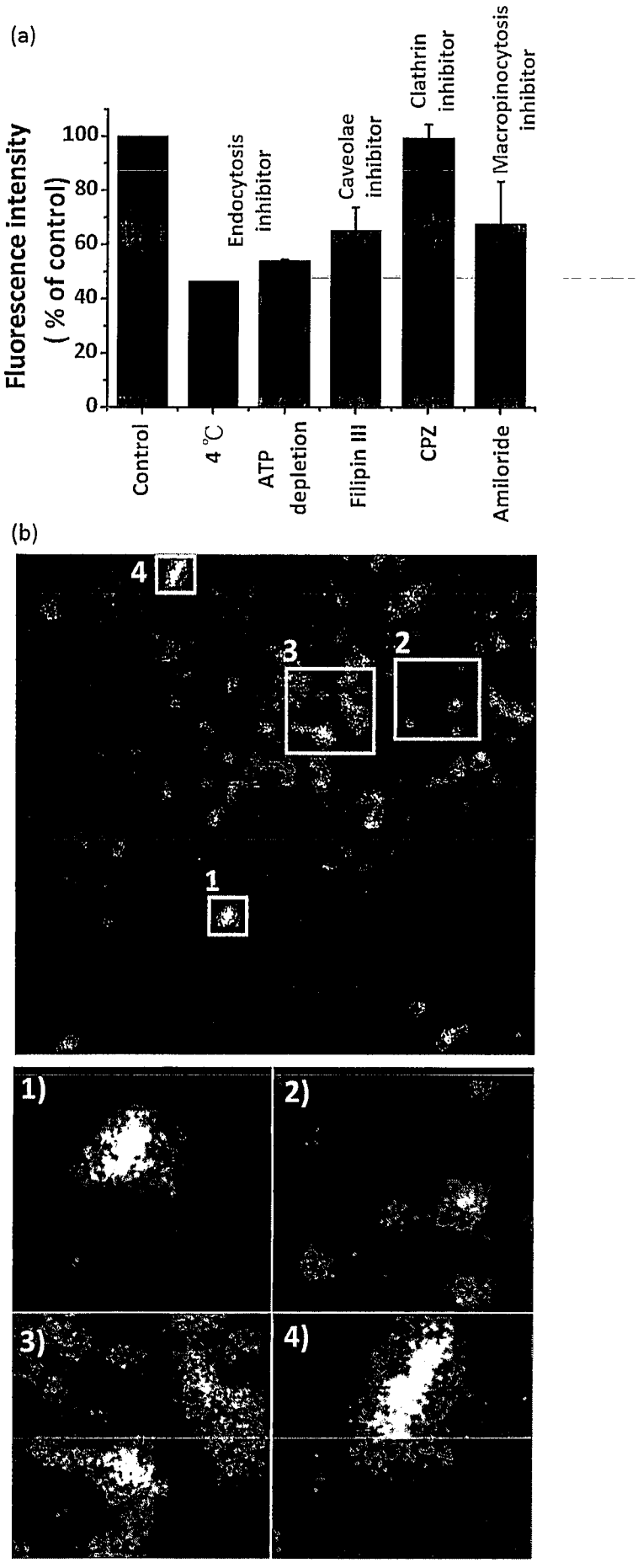
(a)
Fluorescence intensity
(% of control)
100
80
60
40
20
0
Control
4 ℃
ATP depletion
Endocytosis inhibitor
Filipin III
Caveolae inhibitor
CPZ
Clathrin inhibitor
Amiloride
Macropinocytosis inhibitor
(b)
4
3
2
1
1)
2)
3)
4)

Fig 4. (a) Mechanisms of cell uptake of FMSN-TAT-SOD. HeLa cells were pretreated with different pathway inhibitor for 1h, then treated with 50 μg/mL FMSN-TAT-SOD for another 4h in the presence of various types of inhibitors. (b) Super-resolution localization microscopy images the distribution of co-delivery of FMSN-TAT-SOD and FMSN-TAT-GPx in HeLa cells. α-tubulin (Alexa fluor 647-labeled, blue), FMSN-TAT-SOD (FITC-labeled, green) and RMSN-TAT-GPx (RITC-labeled, red). The yellow color indicates colonialization of TAT-SOD and TAT-GPx.

	DLS (nm)			Zeta (mV)	Ni	Protein
	H_2O	PBS	DMEM	H_2O	-	
FMSN-NTA	277.6(32.3)	889.2(125.4)	974.4(112.6)	19.3(0.2)	-	-
FMSN-NTA-Ni^{2+}	361.4(16.7)	900.2(19.9)	1058.5(20.5)	-1.8(0.6)		-
FMSN-SOD	599.3(49.2)	662.7(62.9)	522.3(93.3)	-8.38(0.3)	0.6%	1.19%
FMSN-GPx	557.4(1.0)	646.5(113.3)	661.6(61.6)	-7.49(0.1)		1.22%

Table S1. Physical properties of nanoparticles. Dynamic light scattering (DLS) for particle sized and zeta potential for surface charge in different solutions. Nickel content is determined by ICP-MS and protein amount is quantified by Bradford assay.

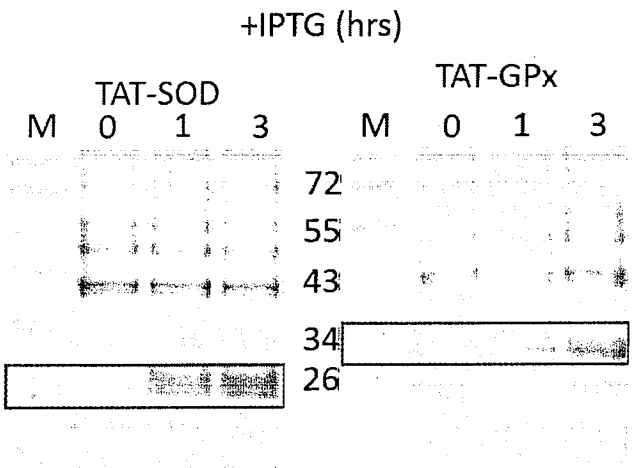

Figure S1. TAT-fusion protein overexpression. TAT-SOD and TAT-GPx proteins were overexpressed from pQE-TAT-vectors by IPTG induction within 0, 1, 3 hr in E. coli express system.

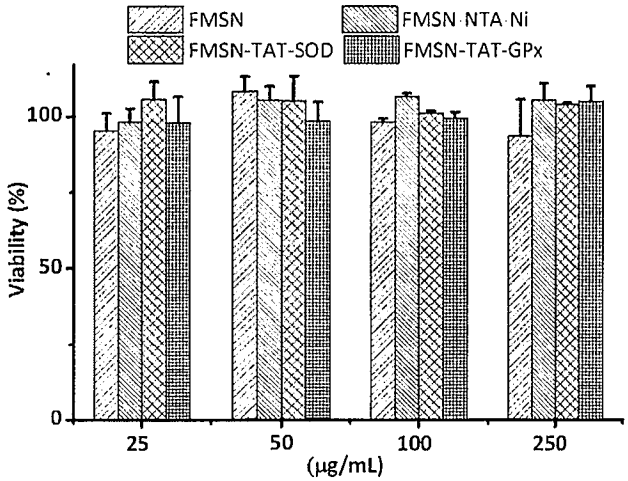

Figure S2. Cytotoxicity of FMSN-TAT-SOD and FMSN-TAT-GPx with different concentrations on HeLa cells by using WST-1 assay

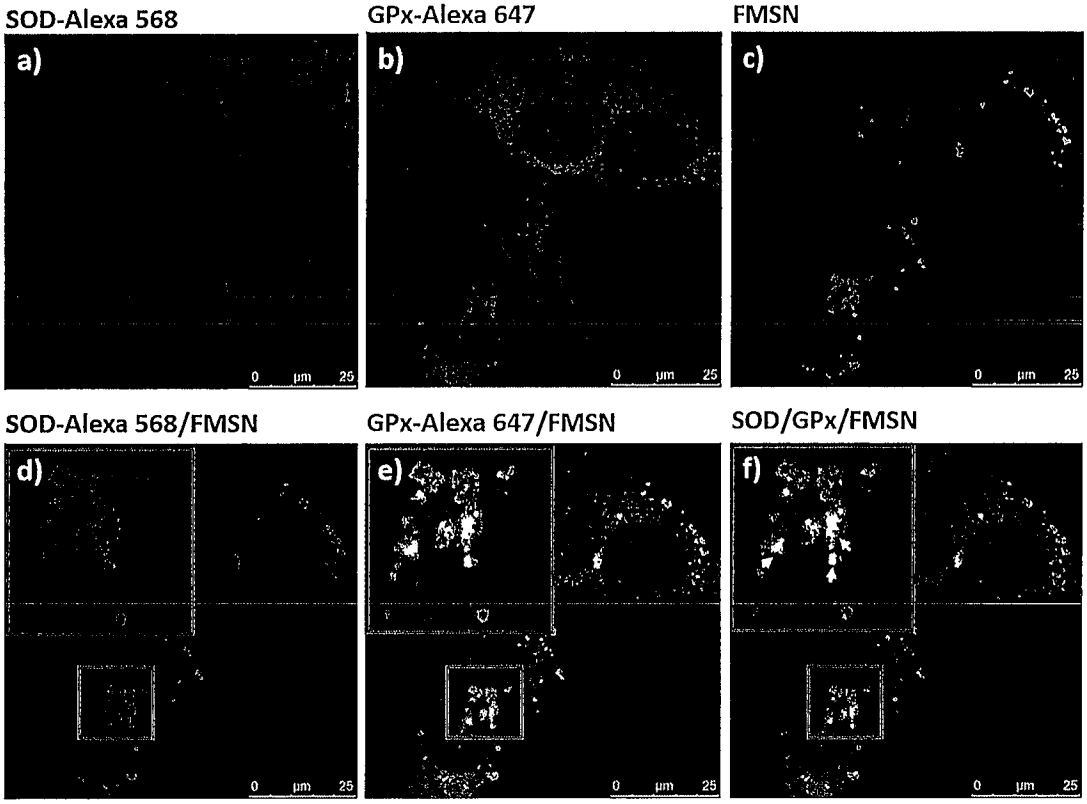

Figure S3. Confocal microscopy images. (a-c) Intracellular distribution of SOD, GPx and nanoparticles. (d) Co-localization of SOD and FMSN (cyan). (e) Co-localization of GPx and FMSN (yellow). (f) Co-localization of SOD, GPx and FMSN (White).

103年度 【 中孔洞二氧化矽奈米粒子與血液 】2年期經費核定總表

執行機構：國立臺灣大學　　主 持 人：牟中原　　教授(凝態科學研究中心)

年 度	業 務 費	研究設備費	國外差旅費	吳大猷獎	管 理 費	合 計	繳交報告時間 報 告 種 類
103	1,228,000	700,000	100,000	--------	284,000	2,312,000	104年5月底前 期中進度報告
104	1,908,000	--------	100,000	--------	286,000	2,294,000	105年10月底前 期末報告
合 計	3,136,000	700,000	200,000	--------	570,000	4,606,000	
全程執行期限： 103/12/01 ～ 105/07/31			計畫編號：MOST 103-2113-M-002 -021 -MY2				

研究類型：一般型研究計畫(個別型)　　學門名稱：無機化學　　流水號：103WFA0150660
研究性質：應用研究　　承辦人：高世平
研究成果歸屬：國立臺灣大學
各項費用之支用請依「科技部補助專題研究計畫經費處理原則」規定辦理。

【 中孔洞二氧化矽奈米粒子與血液(1/2) 】第1年經費清單

執行機構：國立臺灣大學　　主 持 人：牟中原　　教授(凝態科學研究中心)

補助項目	申請金額	核定金額	說明
業務費	2,779,459	1,228,000	一、研究人力費：528,000元 1. 碩士班研究生研究助學金3名144,000元 2. 博士班研究生獎助金2名384,000元 二、耗材、物品、圖書及雜項費用：700,000元(含貴儀中心儀器使用費) 三、本計畫彈性支用額度為25,000元
研究設備費	1,710,000	700,000	高速離心機
國外差旅費	200,000	100,000	一、出席國際學術會議：100,000元 二、本項目不核列管理費
管理費	516,919	284,000	
合　　計	5,206,378	2,312,000	
執行期限：103/12/01 ～ 105/07/31			計畫編號：MOST 103-2113-M-002 -021 -MY2

研究類型：一般型研究計畫(個別型)
貴儀中心使用額度：1,000,000元

【 中孔洞二氧化矽奈米粒子與血液(2/2) 】第2年經費清單

執行機構：國立臺灣大學　　主 持 人：牟中原　　教授(凝態科學研究中心)

補助項目	申請金額	核定金額	說明
業務費	4,560,632	1,908,000	一、研究人力費：1,008,000元 1. 碩士班研究生研究助學金2名144,000元 2. 博士班研究生獎助金3名864,000元 二、耗材、物品、圖書及雜項費用：900,000元(含貴儀中心儀器使用費) 三、本計畫彈性支用額度為25,000元
研究設備費	1,400,000	0	
國外差旅費	200,000	100,000	一、出席國際學術會議：100,000元 二、本項目不核列管理費
管理費	784,095	286,000	
合　　計	6,944,727	2,294,000	
執行期限：104/08/01 ～ 105/07/31			計畫編號：MOST 103-2113-M-002 -021 -MY2

研究類型：一般型研究計畫(個別型)
貴儀中心使用額度：1,000,000元